Universidade do Algarve

Instituto Superior de Engenharia

Non Chemical Natural Organic Matter Removal with a Contact TiO_2 Process

André Martins Ramos

Dissertation to obtain the degree of

Master of Food Technology

Supervisors (Cranfield University):
Prof. Bruce Jefferson
Dr. Peter Jarvis

Supervisors (Algarve University):
Prof. Ana Cristina Figueira

Faro
2014

Universidade do Algarve

Instituto Superior de Engenharia

Non Chemical Natural Organic Matter Removal with a Contact TiO_2 Process

André Martins Ramos

Dissertation to obtain the degree of

Master of Food Technology

Supervisors (Cranfield University):
Prof. Bruce Jefferson
Dr. Peter Jarvis

Supervisors (Algarve University):
Prof. Ana Cristina Figueira

Faro
2014

Universidade do Algarve

Instituto Superior de Engenharia

Non Chemical Natural Organic Matter Removal with a Contact TiO_2 Process

Declaração de autoria de trabalho

Declaro ser a autor deste trabalho, que é original e inédito. Autores e trabalhos consultados estão devidamente citados no texto e constam da listagem de referências incluída.

_____

Andre Martins Ramos

Faro
2014

Acknowledgments

This Master research has been carried out within the Cranfield Water Institute at Cranfield University, United Kingdom.

I wish to thank all the persons belonging to these institutions who contributed to this work.

I want to thank to Prof. Bruce Jefferson, Dr. Peter Jarvis, Dr. Ana Cristina Figueira for the continuous support during all the phases of this project through very stimulating and enlightening discussions, field work and daily encouragements. I am grateful for all the contributions of time, ideas and insight in all circumstances that definitely contributed to the completion of this project.

I would like to express my gratefulness to Dr. Oliver Autin who provided extremely important support in crucial periods of this project. With his calm and professionalism, his supervision always resulted in rich and efficient exchanges.
Miscellaneously, I would like to thank to technical staff, Jane Hubble, Rukhsana Ormesher, Alan Nelson and Christine Kimpton for their help in work lab.

It is a pleasure to thank all the students from the CWI who made this Master Research possible and particularly to Tomas Molnar, Dr. Ana Soares, Dr. Antonio Guerreiro, Francisco Simões, Dr. Catarina Henrique, Dr. Tamas Zsirai, Zhao Zhao, Dr. Joao Souza and Martina Santinelli.

I would like to express also my gratefulness to my special friends Tomas Mólnar, Tamas Zsirai, Francisco Simões, Yerbol Sarbassov, Dr. Joao Souza and Martina Santinelli for the funny moments

I have the chance to have a wonderful and understanding family. Thanks to Fernando Ramos (Dad) and Anabela Ramos (Mom) for your moral support and encouragements along the course of this time in England.

"A drop of water is worth more than a sack of gold to a thirsty man" ***unknown***

Resumo

Ramos, A. M. (2014). *Remo*ção *de* matéria orgânica *natural através de adsor*ção *em dióxido de titânio imobilizado em fluropolimeros***.** Dissertação de Mestrado em Tecnologia de Alimentos. Universidade do Algarve. Faro, Portugal.

A produção de água potável a partir de águas naturais superficiais requer a utilização de tecnologias adequadas para uma eficiente remoção de matéria orgânica natural, assim como outros contaminantes. O grande problema do tratamento de água potável está relacionado com a presença de matéria orgânica dissolvida, que em concentrações elevadas, aumenta a necessidade de um aumento de adição de coagulantes, reage com o cloro da desinfeção produzindo sub-produtos clorados, que consequentemente podem promover um aumento no crescimento de bactérias no decurso da distribuição.

A matéria orgânica natural é um termo utilizado para designar todos os compostos orgânicos provenientes de plantas e animais presentes no meio ambiente. Existe uma grande diversidade de substâncias húmicas e não-húmicas nos solos, sedimentos e águas naturais. As características da matéria orgânica natural são influenciadas basicamente por processos biogeoquímicos e envolvidos no ciclo do carbono, tanto no meio terrestre como no meio aquático.

Os componentes principais da matéria orgânica natural são essencialmente substâncias húmicas classificadas como ácido húmico, ácido fúlvico e humina. Estas substâncias húmicas, devido á sua natureza ubíqua têm um papel fundamental no transporte e ligação de poluentes naturais, atuando como percursores de produtos carcinogénicos provenientes da desinfeção durante o processo de cloração nas estações de tratamento de agua potável.

Existem vários estudos para remoção de matéria orgânica natural através da adsorção em diferentes sólidos adsorventes, como carbono ativado, minerais e kaolinite.

Recentemente, a remoção de matéria orgânica natural de água potável através de processos avançados de oxidação, tem atraído grande interesse, pois trata-se de um processo sustentável que proporciona a mineralização da maioria dos contaminantes orgânicos, isto é, os compostos não são apenas adsorvidos mas transformados em CO_2, H_2O e aniões inorgânicos.

Existem diferentes processos avançados de oxidação, desde a reação de Fenton, ozonização e a fotocatálise por dióxido de titânio, no entanto a propriedade química comum nestes processos é a capacidade de gerar radicais hidroxilo (•OH).

As limitações da aplicação do dióxido de titânio em processos de tratamento de água residem essencialmente no pós-tratamento, nomeadamente na separação de nanopartículas de TiO_2 altamente dispersas. Para resolver estas limitações, muitos estudos têm sido realizados para imobilizar o TiO_2 em várias matrizes utilizando diferentes métodos.

Neste trabalho pretende-se criar um meio imobilizando o TiO_2 em diferentes polímeros (fluoropolímeros) através de fotocatálise, usando uma recção denominada de PSFD. Os fluoropolímeros utilizados foram o fluoreto de polivinilideno (PVDF) e o politetrafluoretileno (PTFE) também conhecido como Teflon.

As primeiros imagens através do microscópio eletrônico foi possivel observar uma melhor cobertura de TiO_2 na superfíce do polímero PVDF comparado com o PTFE (Figuras 4.3 e 4.4). Por esta razão o PVDF foi utilizado para a continuação do trabalho experimental.

Após reação de PSFD, foi possivel verificar que a extensão da cobertura de TiO_2 na superfície de PVDF pode ser controlada atraves de pH. As figuras 4.8 a 4.12 mostram que em meio ácido existe maior quantidade de TiO_2 na superfície de PVDF comparado com o meio básico.

Para a avaliar a capacidade de fotodegradação, submeteu-se o meio $PVDF^f$-TiO_2 preparado em diferentes soluções de TiO_2, de concentração 0.5, 1.5 e 2.5 g/L com diferentes pH (1,3,5,7 e 10). As figuras 4.14 a 4.17 mostram a curva de degradação do azul metileno. Apenas foram feitos estudos de cinética no meio preparado em meio ácido. Na tabela 4.1 é possível verificar que $PVDF^f$-TiO_2 preparado com uma solução de TiO_2 1.5g/L a pH 3, apresenta um capacidade de degradação de azul metileno de 97.58% apos 70 minutos, uma constante de pseudo primeira ordem de 0.054 min^{-1} e um tempo de meio vida de 12.85 minutos. Segundo as imagens SEM e os resultados de fotodegradação considerou-se serem as melhores condições de preparação para desenvolver o meio para estudos de adsorção.

Em seguida, este meio foi testado em sucessivos testes Jar (300 rpm durante 10 minutos) seguido de fotodegradações de azul de metileno para verificar a robustez do meio, em relação ao tipo de ligação do TiO_2 e o polímero PVDF. Os resultados indicam que existe uma forte atracção electrostática entre o TiO_2 e PVDF, pelo que foi

confirmado pelas figura 4.22 e as constantes de pseudo primeira ordem expressas na tabela 4.2.

Após desenvolvimento do meio $PVDF^{f}$-TiO_2 optimizado, este foi utilizado para adsorver ácido húmico como composto representante de matéria orgânica natural. Foi utilizado tambem TiO_2 em pó para adsorver HA de forma a comparar as isotermas de adsorção e a assim chegar a um valor em massa de TiO_2 na superfície do polímero PVDF (0.813mg de TiO_2 por grama de PVDF)(Tabela 4.6).

A isoterma de adsorção de TiO_2 em pó com HA é do tipo de Langmuir.

Em relação ao meio $PVDF^{f}$-TiO_2 a adsorção de HA segue os modelos de Freundlich e Langmuir.

Os resultados da linerarização de Langmuir indicam uma capacidade de adsorção de 0.014 mg de HA por grama de PVDF. A constante b de Langmuir indica uma afinidade de 0.184 L/mg. (Tabela 4.4) Os valores R_L abaixo de 1 indicam que a adsorção de ácido húmico em $PVDF^{f}$-TiO_2 é favorável (Tabela 4.5)

Em relação a linerarização de Freundlich, os parametros indicam uma capacidade adsortiva de 0.0019 (L/mg) e uma intensidade (*n*) de 1.44, o que significa uma adsorção favorável (Tabela 4.4).

Baseado na isoterma de adsorção de ácido húmico no meio $PVDF^{f}$-TiO_2 foram efectuados 8 ciclos de adsorção e seguido de 120 minutos de regeneração do meio por luz UV entre ciclos.

De acordo com a figura 4.35, o meio $PVDF^{f}$-TiO_2 mantém a sua estabilidade de adsorção durante os 8 ciclos pois as curvas de adsorção são muito semelhantes.

Na figura 4.36 é possível verificar que o meio $PVDF^{f}$-TiO_2 mantém a sua capacidade de adsorção, com um valor médio de 0.014 mg de HA por grama de $PVDF^{f}$-TiO_2.

De acordo com estes resultados experimentais, procedeu-se ao desenvolvimento de uma coluna de adsorção para avaliar futura aplicação na índustria da água.

Uma solução de HA (5 mg/L) foi introduzida na coluna no sentido ascendente com diferentes caudais 10.40, 5.19, 3.25, 2.60, 1.30 mL/min.

A figura 4.37 mosta as curvas de ruptura onde é possivel verificar que a medida que aumenta o caudal diminui a remoção de HA. Através do tratamento de resultados a melhor remoção de HA é de 0.42% para um caudal de 1.30 mL/min (Tabela 4.7).

Abstract

Ramos, A. M. (2014). *Non chemical natural organic matter removal with a contact TiO_2 process***.** Master in Food Technology. Algarve University, Faro, Portugal.

The current work looked for a new media to remove natural organic matter by adsorption on TiO_2 nanoparticles bound to fluoropolymers beads through photocatalysis. The work investigated the best methods of production as well the effectiveness of the media thus providing insight into its potential for further adsorption technology development.

The results obtained lead to the conclusion that is possible to immobilize TiO_2 on a PVDF surface by UV-V, resulting in a photocatalytic surface deposition functionalization. The extended of the PSFD reaction can be controlled by adjusting the pH, with acidic conditions increasing the extension of surface coverage.

The polymer with significant results was PVDF, based on SEM figures, MB photodegradation (97.58 %), K_{app} (0.054 min^{-1}) and $t_{1/2}$ (12.85 min) the optimum conditions to increase surface coverage of PVDF is a solution of 1,5 g/L of TiO_2 pH 3 under 2 h on UV collimated beam.

The photocatalytic activity of $PVDF^f$-TiO_2 following Jar tests suggests a very strong electrostatic bond between the TiO_2 and the polymer surface.

The adsorption of HA onto $PVDF^f$-TiO_2 was found to be well described by both the Langmuir and Freundlich models. The maximum adsorption capacity (q_{max}) was 0.0149 mg/g and the parameters *n* and K_L show a favorable adsorption.

Fixed-bed adsorption column studies was developed to remove HA from water, using a fixed bed height of 17 cm, a fixed feed concentration of 5mg/L but different flow rates. Results show that for lower flows there is a higher removal as compare with a higher flow. The best result obtained was 0.42% of HA removal with a feed flow of 1.30 mL/min.

Index

Acknowledgments....7

Resumo....9

Abstract....13

Figures Index....18

Tables Index....21

Glossary....22

1. Literature review....24

1.1. Drinking water and natural organic matter (NOM)....24

1.2. Removal of NOM by Advanced Oxidation Processes (AOPs)....24

1.2.1. Heterogeneous photocatalysis....25

1.2.2. TiO_2 Photocatalysis....26

1.2.3. Photoxidation of pollutants....29

1.3. Adsorption....30

1.3.1. Langmuir isotherm....31

1.3.2. Freundlich isotherm....32

1.3.3. Humic acid removal by adsorption....33

1.4. Immobilization of Titanium dioxide....34

1.4.1. Polyvinylidene fluoride....34

1.4.2. Polytetrafluoroethylene....35

1.5. Scanning electronic microscopy (SEM)....35

1.6. Fixed - bed Adsorption column....36

1.6.1. Analysis of column data....37

2. Aims of the present work....38

3. Materials and Methods....39

3.1. Materials....39

3.1.1. Polymers....39

3.2.2. Chemicals reagents....39

3.2.3. Instrumentation 39
3.2. Methods 41
3.2.1. Media preparation 41
3.2.2. Media performance 42
3.2.3. Adsorption experiments 43
4.1 Media preparation 47
4.1.1. Observation of PVDF and PTFE surfaces under SEM 47
4.1.2. Photocatalytic surface functionalization deposition of TiO_2 into PVDF and PTFE surfaces 48
4.1.3. Influence of UV light distance (100 mm e 230 mm) 50
4.1.4. Scanning electron microscopic images of $PVDF^f$-TiO_2 at different pH 51
4.2. Media Performance 55
4.2.1. Photodegradation of methylene blue using $PVDF^f$ - TiO_2 prepared at different concentrations and pH of TiO_2 solutions 55
4.2.2. Evaluation of photocatalytic activity of $PVDF^f$-TiO_2 after centrifugations in Jar test apparatus 62
4.2.3. Blanks 64
4.3. Humic acid adsorption 67
4.3.1. Adsorption isotherm of humic acid on TiO_2 powder 67
4.3.2. Adsorption isotherm of humic acid on $PVDF^f$ - TiO_2 media prepared with optimized conditions (1.5 g/L, pH=3) 68
4.3.3. Calculation of the mass TiO_2 per gram of PVDF based on adsorption capacities 72
4.3.4. Blanks 73
4.5. Photodegradation and adsorption of humic acid in $PVDF^f$ - TiO_2 media 73
4.5.1. Determination of regeneration time 73
4.5.2. $PVDF^f$- TiO_2 Adsorption stability 75
4.6. Adsorption column 76
5. Conclusion 78

6. Suggestions for future work 79
7. References 80
8. Annex.....88

Figures Index

Figure 1.1 – Schematic photo-excitation in a semiconductor particle	*26*
Figure 1.2 – Schematic illustration for energetics and primary reaction mechanism of TiO_2 photocatalysis	*28*
Figure 1.3 – Adsorption mechanism	*30*
Figure 1.4 – Chemical structure of PVDF	*34*
Figure 1.5 – Chemical structure of PTFE	*35*
Figure 1.6 – Example of a breakthrough curve	*37*
Figure 3.1 – Collimated beam UV light reactor a) and associated controller b)	*39*
Figure 3.2 –Scanning electron microscope (SEM)- Philips/FEI XL 30 SFEG	*40*
Figure 3.3 – Photodegradation of Methylene Blue	*42*
Figure 3.4 –Fixed-Bed adsorption column	*45*
Figure 3.5 – Schematic overview of the adsorption column – A) Fixed-bed adsorption column B) Outlet container C) Watson Marlow 520S pump, UK D) Inlet container (Feed concentration of HA = 5 mg/L)	*46*
Figure 4.1 – PVDF surface (x5000)	*47*
Figure 4.2 – PTFE surface (x5000)	*47*
Figure 4.3 – Scanning electron microscopic image of $PVDF^f$-TiO_2 prepared with a 1.5 g/L TiO_2 solution at pH 3 (UV time = 2h, light distance = 100mm) (x5000)	*48*
Figure 4.4 – Scanning electron microscopic image of $PTFE^f$-TiO_2 prepared with a 1.5 g/L TiO_2 solution at pH 3(UV time = 2h, light distance = 100mm) (x5000)	*48*
Figure 4.5 – Scanning electron microscopic image of a) PVF b)PVF^f-TiO_2 prepared at pH 5 (external side) c) PVF^f-TiO_2 prepared at pH 5 (internal side)	*49*
Figure 4.6 – Scanning electron microscopic image of $PVDF^f$-TiO_2 prepared with a 1.5 g/L TiO_2 solution at pH 3(UV time = 2h, light distance = 100mm) (x5000)	*50*
Figure 4.7 – Scanning electron microscopic image of $PVDF^f$-TiO_2 prepared with a 1.5 g/L TiO_2 solution at pH 3(UV time = 2h, light distance = 230mm) (x5000)	*50*
Figure 4.8 – PVDF surface after PSFD with TiO_2 (1.5 g/L at pH = 1) (x5000)	*51*
Figure 4.9 – PVDF surface after PSFD with TiO_2 (1.5 g/L at pH = 3) (x5000)	*52*
Figure 4.10 – PVDF surface after PSFD with TiO_2 (1.5 g/L at pH = 5) (x5000)	*52*
Figure 4.11 – PVDF surface after PSFD with TiO_2 (1.5 g/L at pH = 7) (x5000)	*53*
Figure 4.12 – PVDF surface after PSFD with TiO_2 (1.5 g/L at pH = 10) (x5000)	*53*
Figure 4.13 – Mechanistic suggestion for TiO_2 photocatalytic surface functionalization	*54*

deposition as function of pH

Figure 4.14 – Photodegradation of Methylene blue – $PVDF^f$- TiO_2 prepared at pH = 1	*57*
Figure 4.15 – Photodegradation of Methylene blue – $PVDF^f$- TiO_2 prepared at pH = 3	*57*
Figure 4.16 – Photodegradation of Methylene blue – $PVDF^f$- TiO_2 prepared at pH = 5	*58*
Figure 4.17 – Photodegradation of Methylene blue – $PVDF^f$- TiO_2 prepared at pH = 7	*58*
Figure 4.18 – Pseudo-first-order kinetics – $PVDF^f$-TiO_2 prepared at pH = 1	*60*
Figure 4.19 - Pseudo-first-order kinetics – $PVDF^f$-TiO_2 prepared at pH = 3	*60*
Figure 4.20 - Pseudo-first-order kinetics – $PVDF^f$-TiO_2 prepared at pH = 5	*61*
Figure 4.21 – Photodegradation of Methylene blue –($PVDF^f$- TiO_2 submitted to three centrifugations	*62*
Figure 4.22- Surface analysis of $PVDF^f$- TiO2 (1.5 g / L prepared at pH = 3) and after three centrifugations. Clockwise from top left: a) x1000 b) x5000 c) x35000 d) x70000	*63*
Figure 4.23– Pseudo-first order kinetics – $PVDF^f$-TiO_2 after three consecutive centrifugations	*64*
Figure 4.24– Blanks tests to assess the photocatalytic capacity of the media $PVDF^f$-TiO_2	*65*
Figure 4.25 –Photodegradation capacity of PVDF +TiO_2 (1.5 g / L pH = 3) a) prepared without UV light (dark) b) and subjected to three consecutive centrifugations.	*66*
Figure 4.26– Surface Analysis of PVDF + TiO_2 (1.5 g / L at pH = 3) a) prepared without UV light b) subjected to three centrifugations	*66*
Figure 4.27– Adsorption isotherm of HA on TiO_2 at pH 5; qe (mg/g) is the concentration of HA adsorbed per gram of TiO_2 determined by UV-Vis spectroscopy at 254 nm; Ce (mg/L) is mass concentration of HA at the equilibrium, according to the Langmuir model	*67*
Figure 4.28–Linear plot of Langmuir isotherm for adsorption of HA onto $PVDF^f$-TiO_2	*68*
Figure 4.29–Adsorption isotherm of HA on $PVDF^f$ - TiO_2; qe (mg/g) is the concentration of HA adsorbed per gram of $PVDF^f$ - TiO_2 determined by UV-Vis spectroscopy at 254 nm; Ce (mg/L) is HA mass concentration at the equilibrium, according to the Langmuir model	*69*
Figure 4.30– Linear plot of Langmuir isotherm for adsorption of HA onto $PVDF^f$-TiO_2	*69*
Figure 4.31– Linear plot of Freundlich isotherm for adsorption of HA onto $PVDF^f$-TiO_2	*71*

Figure 4.32 –Adsorption of humic acid in PVDF polymer pellets and 0,22 μm filters 73

Figure 4.33– Photodegradation of Humic acid with PVDF^{f}-TiO$_2$ media 74

Figure 4.34 – Schematic illustration of the possible structure of meso – TiO$_2$/SAC and adsorption and photocatalytic degradation of HA by meso – TiO$_2$/SAC 74

Figure 4.35 – Adsorption isotherms stability of HA on PVDF^{f}-TiO$_2$ showing 8 cycles with 120 min regeneration time per cycle 75

Figure 4.36 - Adsorption capacity of PVDF^{f}- TiO$_2$ showing 8 cycles with 120 minutes regeneration time per cycle 75

Figure 4.37- Breakthrough curves of HA on PVDF^{f}-TiO$_2$ 77

Figure 8.1 – Humic acid calibration curve 88

Tables Index

Table 4.1 – Photodegradation of methylene blue (%) and Pseudo-first-order kinetics parameters	61
Table 4.2 - Photodegradation (%) and Pseudo-first-order kinetics parameters	64
Table 4.3 –-Adsorption constants for humic acid on TiO_2 according to the Langmuir model	67
Table 4.4– Langmuir and Freundlich constants and regression coefficients for the adsorption of humic acid on the surface of $PVDF^f$-TiO_2	71
Table 4.5 –Dimensionless Constant separation factor R_L for the adsorption of HA on $PVDF^f$-TiO_2	72
Table 4.6–Mass of TiO_2 (mg) per gram of PVDF	72
Table 4.7 – Saturation times and total removals in fixed-bed adsorption column	77

Glossary

AOP – Advanced oxidation process;

b (or Ka) – Langmuir adsorption constant (L/mg)

BSE – Back scatter electron detector

CB – Conduction Band;

Ce - Adsorbate equilibrium concentration (mg/L)

C_i - initial concentration of the reactant (mg/L)

C_0 – Adsorbate initial concentration (mg/L)

C - Concentration of the reactant at time t (mg/L)

EBCT – Empty Bed Contact time (min.)

EDX – Energy dispersive X- ray;

Eg – Band gap Energy

FA – Fulvic acid;

F – Flow of adsorbate (mL/min)

h^+ - Electron holes

HA – Humic acid;

K_f – Freundlich Isotherm constant for adsorption capacity (L/mg)

K_{app} - apparent-first-order rate constant (min^{-1})

m - Adsorbent mass (g)

MB – Methylene blue;

n – Freundlich isotherm constant for adsorption intensity

NOM – Natural organic matter;

PSFD – Photocatalytic surface functionalization deposition;

PTFE – Polytetrafluoroethylene;

PVF – Polyvinyl Fluoride

PVDF - Polyvinylidene fluoride;

$PTFE^{f}$-TiO_2 – Photocatalytic surface functionalization deposition of TiO_2 into PTFE surface;

$PVDF^{f}$-TiO_2 – Photocatalytic surface functionalization deposition of TiO_2 into PVDF surface;

q - Mass of solute adsorbed per mass of adsorbent (mg / g) – adsorption capacity

q_{max} – Maximum adsorption capacity (mg/g)

R^2 – Correlation coefficients

R_L – Separation factor

SE – Secondary electron detector;

SEM - Scanning electron microscope

t = time (min)

$t_{1/2}$ – Half life time (min)

t_b – Breakthrough time (min.)

t_s – Saturation time (min.)

TOC – Total organic carbon

THMFP – Trihalomethane formation potential

UV – Ultraviolet radiation

UVC – Ultraviolet radiation (280-100nm)

UV – V- Ultraviolet/Visible radiation

V - Solution volume (L)

VB – Valence band

VUV – Vacuum ultraviolet radiation

Greek symbols:

h – Planck's constant

v – Frequency

1. Literature review

1.1. Drinking water and natural organic matter (NOM)

The quality of drinking water is a key indicator for assessing the level of development of a country and the welfare of its population.

Disinfection of drinking water is essential to prevent the transmission of diseases, both in developing and industrialized countries. The production of drinking water from natural surface water requires the use of technologies for the efficient removal of natural organic matter (NOM) as well as other contaminants. The major problem of the treatment of drinking water is related to the presence of dissolved organic matter at high concentrations, which increases the need for increased addition of coagulant, which reacts with chlorine disinfection producing chlorinated by-products, which in turn may promote a regrowth of bacteria during the distribution (Humbert et al., 2008).

The NOM is a term applied to all organic compounds from plant or animal origins that are present in the environment. There is a wide variety of humic substances and non-humic soils, sediments in natural waters. The characteristics of NOM are influenced primarily by biogeochemical processes involved in the carbon cycle, both on land and in water (Mori et al., 2013);(Uyguner & Bekbolet, 2004).

The main components of natural organic matter are mainly humic substances classified as humic acid (HA), fulvic acid (FA) and humin. These humic substances, due to its ubiquitous nature, have a key role in the transport and binding of natural pollutants, acting as precursors of carcinogenic products during disinfection, the chlorination steps in drinking water treatment (Uyguner & Bekbolet, 2011).

The humic substances are composed of a variety of aliphatic, aromatic, different functional groups, with and without electric charges, different sizes and molecular structures (Matilainen & Sillanpää, 2010);(Matilainen & Sillanpää, 2011).

1.2. Removal of NOM by Advanced Oxidation Processes (AOPs)

Recently, the removal of NOM from potable water through advanced oxidation processes (AOPs) have attracted a great interest, because it is a sustainable process and provides the majority of the mineralization of organic contaminants, since the compounds are not only adsorbed but also transformed into CO_2, H_2O and inorganic anions (Andreozzi, et

al., 1999).

AOPs are divided in homogeneous processes, where the reactants and catalysts are in the same phase and heterogeneous processes where catalysts and reagents are in different phases. Heterogeneous processes are the most commonly used because it's easier to recover the products from reactants (Goetz et al., 2009).

The results of various studies dealing with NOM removal by AOPs are always study specific depending on the water's characteristics, namely the amount of organic matter. Therefore, the characterization of NOM in water should be made before the design and optimization of the AOP treatment. Furthermore, in order to assess its influence on the downstream processes, it is important to determine the organic characteristics of the treated water (Bundaleski et al., 2010).

AOPs have been studied intensively for decades. Various combinations of oxidants, radiation and catalysts have been developed for the removal of NOM and organic pollutants, e.g. O_3/H_2O_2, UV/ H_2O_2, UV/O_3, UV/TiO_2, Fe^{2+}/ H_2O_2, Fe^{2+}/ H_2O_2 + hv, vacuum ultraviolet (VUV) radiation or ionizing radiation. These processes involve the generation of highly reactive radical intermediates, especially the $^{\bullet}OH$ radical (Bayarri et al., 2007);(Wiszniowski et al., 2003).

1.2.1. Heterogeneous photocatalysis

The heterogeneous photocatalysis involves the activation of a metal oxide semiconductor by a light source (either sunlight or artificial light). These semiconductors when acting as photocatalysts have two energy regions: the region of lower energy, which correspond to the valence band (VB), where the electrons do not a have free movement and the region of higher energy, which is the conduction band (CB) where the electrons are free to move throughout the crystal, producing an electrical conductivity similar to a metal (Goetz et al. 2009); (Mazille et al., 2009); (Shen et al., 2012)

Between these two regions there is a band gap region. The band gap energy (Eg) is the minimum energy required to excite an electron and promote it from the valence band to the conduction band. A schematic representation of the semiconductor particle is represented in Figure 1.1 and shows the absorption of photons with energy higher than the energy of the band gap resulting in the promotion of an electron from the valence band to the conduction band, generating electron holes (h^+) in the valence band. (Oliveira & Silveira, 2011)

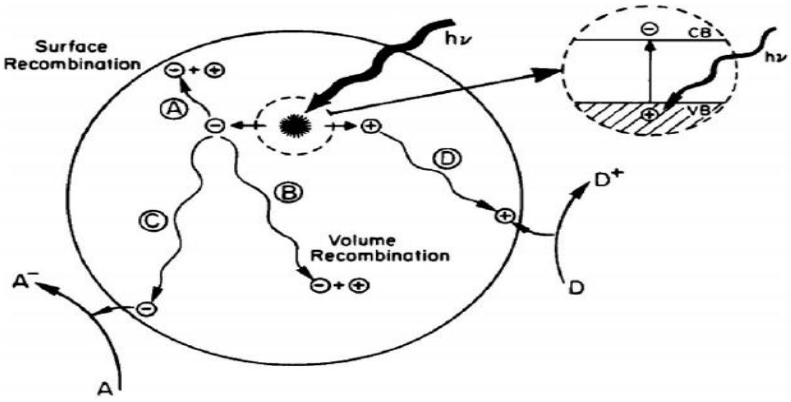

Figure 1.1 – Schematic photo-excitation in a semiconductor particle (Yates, 2009)

1.2.2. TiO_2 Photocatalysis

The Photocatalytic process requires a metallic oxide semiconductor as a catalyst and oxygen as the oxidizing agent. Many metallic oxides have been used; however titanium dioxide has excellent features such as being (Shen et al., 2012);(Gómez-Solís et al., 2012):

a) Photoactive;
b) Excited with visible light and / or ultraviolet light;
c) Biologically and chemically inert;
d) Greater stability;
e) Low cost;
f) Nontoxic;
g) Photo-stable;

This thesis mainly focuses on TiO_2 as a catalyst, the physicochemical properties are summarized in table 1.1 and the data are from supplier AEROXIDE®.

Table 1.1- Physicochemical properties of TiO_2 – Degussa P25

Property	Degussa P-25
Physical state	White powder
Composition	≈ 80 (anatase)
	≈ 20 (rutile)
Density (g L^{-1})	3.8
BET surface area (m^2g^{-1})	≈55
Average primary particle size (nm)	≈30
pH in aqueous solution	3-4
Contents:	
SiO_2 (%)	<0.2
Al_2O_3 (%)	<0.3
Fe_2O_3 (%)	<0.01
TiO_2 (%)	>97
HCl (%)	<0.3
Calcining losses (%)	<2 (1000C)
Porosity	Non-porous
Volatiles (%)	----------

Titanium dioxide when irradiated with electromagnetic radiation with an energy equal or higher to the band gap (Eg = hv ≥ 3.2 eV) begins the process of photoactivation, which generates electron-hole pairs (Equation 1.1). (Houas et al., 2001)

$$TiO_2 \xrightarrow{h\nu} e^- + h^+$$ ***Equation 1.1***

The electrons with high reduction capacity, promote the reduction of dissolved oxygen producing an ion superoxide radical $O_2^{\bullet -}$ and the holes promote the oxidation of adsorbed H_2O and OH^- into the reactive hydroxyl radical ($^{\bullet}HO_{ad}$).(Equation 1.2)(Houas et al., 2001)

$$TiO_2(h^+) + H_2O_{ad} \rightarrow TiO_2 + HO_{ad}^{\bullet} + H^+$$
$$TiO_2(h^+) + HO_{ad}^- \rightarrow TiO_2 + HO_{ad}^{\bullet}$$ ***Equation 1.2***

These reactions are extremely important in the processes of oxidative degradation due

to the high concentration of HO_{ad}^- and H_2O adsorbed on the surface of titanium dioxide particles (Figure 1.2) (Andreozzi et al.,1999)

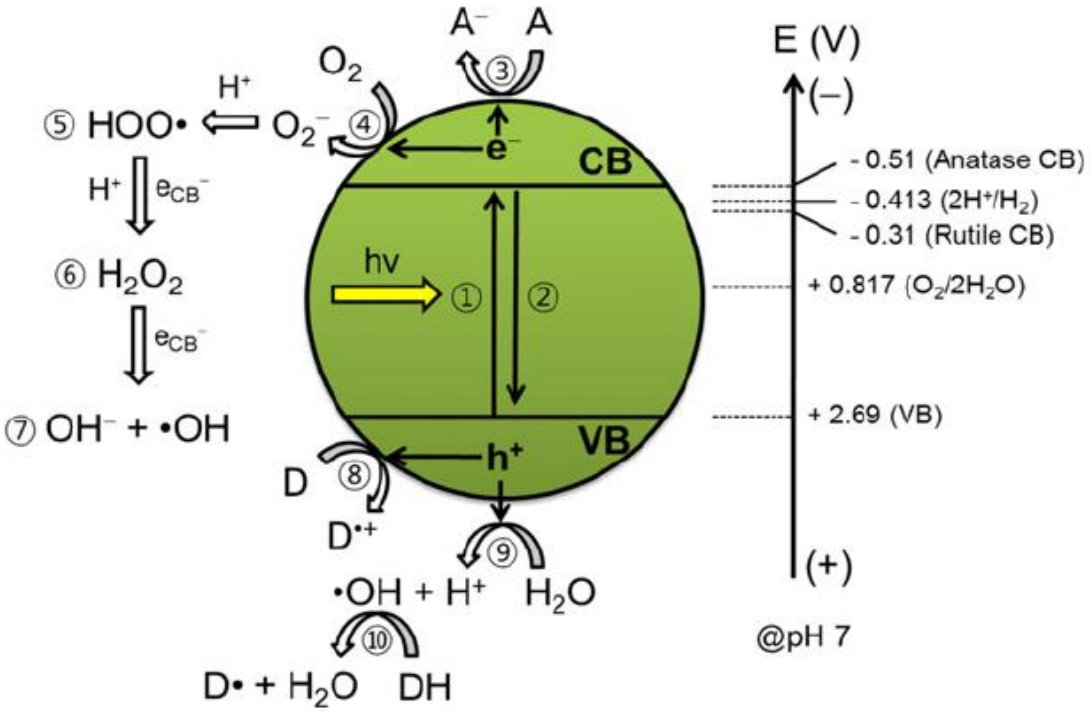

Figure 1.2 - Schematic illustration for energetics and primary reaction mechanism of TiO_2 photocatalysis. 1: Bandgap (E_g) excitation and electron-hole charge pair creation, 2: the charge pair recombination, 3: electron transfer to electron acceptor (A: usually dissolved oxygen), 4: electron transfer to oxygen molecule, 5: formation of hydroxyperoxyl radical via reductive pathaway, 6: formation of hydrogen peroxide, 7: formation of hydroxyl radical, 8: hole transfer to electron donor (D: usually organic pollutants), 9: hole transfer to surface hydroxyl group to generate OH radical, 10: hydroxyl radical-mediated oxidation of organic substrate. Note that the energy levels (right arrow) shift according to the Nernst equation. (Park, et al., 2012)

1.2.3. Photoxidation of pollutants

The photodegradation kinetics of many organic compounds in TiO_2 suspensions under UV illumination has often been modelled to the Langmuir-Hinshelwood mechanism confirming the heterogeneous catalytic character of the system. The Langmuir-Hinshelwood kinetics equation (Equation 1.8) can be expressed as follows (Li et al., 2006) (Kasanen et al., 2011)(Sauer et al., 2002) (Senthilkumaar et al., 2006):

$$\boldsymbol{r = -\frac{dC}{dt} = Kapp.t} \qquad \textbf{Equation 1.3}$$

Integration of this equation will lead to the expected relation of (Pseudo first order reaction equation 1.9):

$$\boldsymbol{\ln C_i/C = K_{app}.t} \qquad \textbf{Equation 1.4}$$

Wherein:
r = pseudo first order rate
C_i = initial concentration of the reactant (mg/L)
K_{app} - apparent-first-order rate constant (min^{-1})
C = concentration of the reactant at time t (mg/L)
t = time (min)

The half-life time (minutes) is the amount of time required to reduce a reactant to half of its initial value and is calculated by equation 1.5 (Bekbolet et al., 2002)

$$\boldsymbol{t_{1/2} = 0.693/K_{app}} \qquad \textbf{Equation 1.5}$$

The titanium dioxide acts as a photocatalyst agent who combines the two reactants (oxygen and light) to promote the degradation of the pollutant. As a definition, photocatalysis is a process in which a chemical reaction is initiated by ultraviolet, visible or infrared light being absorbed by a photocatalyst, promoting a chemical change in the reactants. (Banerjee, Dasgupta, and De 2007);(Bizani et al. 2006);(Q. Li et al. 2011)(Páez et al. 2011). During this process it is important to consider the following steps:

a) Diffusion of reactants dispersed in the solution to the surface of the catalyst;

b) Adsorption of at least one of the reagents;

c) Reaction in the adsorption phase;

d) Removal of products from the interface;

Therefore adsorption and photocatalysis are highly interrelated because both occur on the surface of the particles (Silva, 2008)

1.3. Adsorption

Adsorption is a phase transfer process which is widely used to remove substances from a fluid (either gas or liquid). The definition includes deposition adsorption / enrichment of a chemical species from a fluid phase to the surface of a liquid or solid. In water treatment, adsorption is widely used as a process for removing a variety of solutes. Molecules or ions are removed from an aqueous phase by adsorption on solid surfaces. These surfaces are characterized by strong active sites capable of interacting with solutes in the aqueous phase due to their specific electronic and spatial properties (El-Sharkawy et al., 2007).

According to the adsorption theory, the solid material that provides the surface for adsorption is referred to as adsorbent; the species that will be adsorbed is named adsorbate (Figure 1.3). By changing the conditions of the liquid phase (e.g. concentration, temperature, pH) the adsorbed species can be released from the surface and transferred back into the liquid phase. This reverse process is referred to as desorption (Kaewprasit et al., 1998).

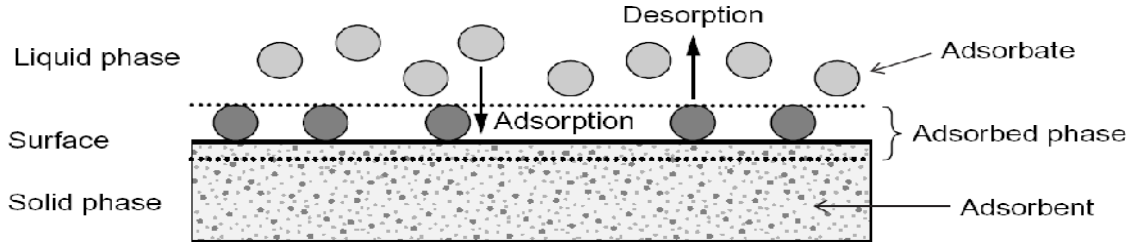

Figure 1.3 – Adsorption mechanism (Worch 2012)

There are different models to describe the adsorption mechanism. In the present work two methods were used to describe the experimental data: Freundlich and Langmuir (Valente et al., 2006); (Xue et al., 2011)

The amount of adsorbed substance (q_e) is calculated using Equation 1.6 as described below:

$$q_e = \frac{(C_o - C_e)}{m}.V \qquad \textbf{Equation 1.6}$$

q_e = mass of solute adsorbed per mass of adsorbent (mg / g) – adsorption capacity

C_0 = adsorbate initial concentration (mg/L)

Ce = adsorbate equilibrium concentration (mg/L)

V = solution volume (L)

m = adsorbent mass (g)

The Langmuir isotherm (Equation 1.7) and Freundlich isotherm models (Equation 1.8) can be used to describe the experimental data obtained from the adsorption curve.

1.3.1. Langmuir isotherm

The Langmuir isotherm assumes monolayer adsorption onto a surface containing a finite number of adsorption sites of uniform strategies with no transmigration of adsorbate in the plane surface. Once a site is filled, no further sorption can take place at that site. This indicates that the surface reaches a saturation point where the maximum adsorption of the surface will be achieved (Khezrianjoo & Revanasiddappa, 2012);(Wan Ngah et al., 2008)

The nonlinear form of the Langmuir is represented by Equation 1.7:

$$q_e = \frac{q_{max}.b.C_e}{1 + b.C_e} \qquad \textbf{Equation 1.7}$$

The linear plot of specific adsorption (Ce/qe) against the equilibrium concentration (Ce) is represented by Equation 1.8:

$$\frac{C_e}{q_e} = \frac{1}{q_{max}.b} + \frac{1}{q_{max}}.C_e \qquad \textbf{Equation 1.8}$$

Wherein:

q_e = mass of solute adsorbed per mass of adsorbent (mg / g);

Ce = adsorbate equilibrium concentration (mg/L)

q_{max} = constant that represents the monolayer deposited per g adsorbent (mg of adsorbate per gram of adsorbent) – Adsorption capacity

b = Ka = adsorption equilibrium constant (known as the Langmuir adsorption constant) related to the affinity of the binding sites (L/mg)

Using Langmuir constant (b), a dimensionless constant termed as separation factor R_L could be calculated according to Equation 1.9:

$$\mathbf{R_L = 1/ (1 + b.C_0)} \qquad \textbf{Equation 1.9}$$

Where C_0 is the initial concentration of adsorbate in water (mg/L). Depending on the values of R_L, the adsorption can be favorable, unfavorable or irreversible. The values of R_L from 0 to 1 are favorable. When a value is greater than 1 the adsorption is unfavorable and zero signifies an irreversible adsorption. (Dutta et al., 2009)

1.3.2. Freundlich isotherm

The Freundlich isotherm assumes the existence of a multilayer structure and provides an exponential distribution of various adsorption sites with different energies. It is used to describe the equilibrium in heterogeneous surfaces and does not assume monolayer adsorption. (Chen et al., 2012);(Tahiri Alaoui et al., 2009);(Xue et al., 2011)

The nonlinear form of the Freundlich model is represented by Equation 1.6:

$$q_e = K_f \ .C_e^{1/n} \qquad \textbf{Equation 1.10}$$

The linear plot of specific adsorption (log q_e) against the equilibrium concentration (log Ce) is represented by Equation 1.7:

$$\log q_e = \log K_f \ + \frac{1}{n} \log .C_e \qquad \textbf{Equation 1.11}$$

Representing graphically log q_e vs. log C_e, we obtain a straight line where 1/n is the slope and log K_f is the intercept.

Wherein:

q_e = mass of solute adsorbed per mass of adsorbent (mg / g);

Ce = adsorbate equilibrium concentration (mg/L)

K_f = Freundlich isotherm constant for adsorption capacity (L/mg)

n = Freundlich isotherm constant for adsorption intensity

Freundlich constants, K_f and *n* correspond to the adsorption capacity and the adsorption intensity, respectively. The higher the value of K_f is the higher is the adsorbent loading that can be achieved. The *n* value indicates the degree of nonlinearity between the solution concentration and the adsorption, as follows: if n=1, then adsorption is linear; if $n<1$, then adsorption is a chemical process; if $n>1$, then adsorption is a physical process (Doulia et al. 2009);(Dutta et al. 2009); (Gürboğa and Tel., 2005); (Tahiri Alaoui et al. 2009).

1.3.3. Humic acid removal by adsorption

Among processes employed in water treatment, adsorption is an important method with high removal efficiency and no harmful by-products. Many kinds of adsorbents have been developed for the removal of humic acid from water. Previous research has suggested that activated carbon (Goetz et al., 2009), as well as resins (Humbert et al., 2008) and biopolymers (chitosan) (Matilainen et al., 2011), can be reasonably used in order to remove humic acid from water. Activated carbon exhibits a high surface area and a high adsorption capacity but it is very expensive, has high operation costs, and requires frequent regeneration. Recently the usage of natural mineral sorbents for wastewater treatment is increasing because of their abundance and low price (Matilainen et al., 2011)(Humbert et al. 2008)(Qi et al., 2008).

Among these adsorbents, nano scaled TiO_2 appears to be a more prominent adsorbent, due its regenerative characteristics. The TiO_2 could be simply regenerated by UV light irradiation via photocatalytic oxidation process for reuse. However, it is very difficult to recover the nano scaled TiO_2 from treated water, due the size limitation. Some researchers have reported the use of nano structured TiO_2 microsphere to be incorporated with membrane filtration for drinking water production. This hybrid process could provide the drinking water with high quality to meet the stringent drinking water standards and lower the overall water treatment costs. Such hybrid membrane is able to retain the saturate TiO_2 microsphere adsorbent which prevents fouling caused by HA and at the same time, upon UV irradiation, the photocatalytic TiO_2 microsphere is able to oxidize HA and thus be regenerated for further use (Xue et al., 2011); (Peng et al., 2012); (Mazille et al., 2009 a))

This thesis follows the same principle but uses TiO_2 immobilized by photocatalysis in fluoropolymers.

1.4. Immobilization of Titanium dioxide

The limitations of applying titanium dioxide in water treatment processes lies essentially in the post-treatment, particularly in the separation of highly dispersed TiO_2 nanoparticles. To address these limitations, many studies have been conducted to immobilize the TiO_2 into various solid matrices by different methods (Mazille et al., 2009 b).

Matrices such as polymers, fibers, glass beads and ceramic materials are used to immobilize the TiO_2 using the sol-gel method. (Hwang et al., 2012)(Mazille et al., 2009 a);(Mori et al., 2013);(Shen et al., 2012)

Mazille et al, 2009 a), report the immobilization TiO_2 in PVF films by photocatalytic surface functionalization deposition (PSFD). In this work it is intended to immobilize the TiO_2 by PSFD into different fluoropolymers beads rather on films, to increase the surface area for HA adsorption. The fluoropolymers used were the Polyvinylidene fluoride (PVDF) and Polytetrafluoroethylene (PTFE).

The immobilization of TiO_2 into fluoropolymers can be evaluated by Scanning electron microscope (SEM) and by the photocatalytic and adsorption capacity with the reaction rate varying proportionally with the coverage (Chen et al., 2007)(Li et al., 2006)(Xue et al., 2011).

1.4.1. Polyvinylidene fluoride

Polyvinylidene fluoride or polyvinylidene difluoride (PVDF) is a partially fluorinated homopolymer which is made by polymerizing vinylidene monomer. The repeat unit is shown below in figure 1.4:

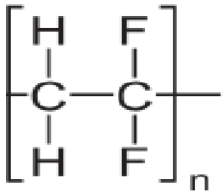

Figure 1.4 –Chemical structure of PVDF (Polymers database, Polymers 2013 Copyright)

PVDF is a specialty plastic material in the fluoropolymer family; it is used generally in applications requiring the highest purity, strength, and resistance to solvents, acids, bases and heat and low smoke generation during a fire event. Compared to other fluoropolymers, it has an easier melt process because, of its relatively low melting point of around 177 °C.

(Polymers database, Polymers 2013 Copyright, Available in: www. Polymersdatabase.com)

1.4.2. Polytetrafluoroethylene

PTFE which is also known as Teflon is a thermoplastic polymer. It is formed by the radical polymerization of tetrafluoroethyelene. The outside of the polymer consists of a layer of fluorine atoms which repel all other molecules. It is used as the coating in nonstick pans and as a bearing that needs no lubrication. (Polymers database, Polymers 2013 Copyright, Available in: www. Polymersdatabase.com)

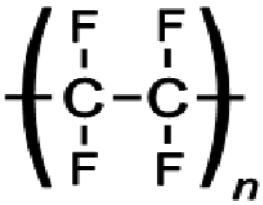

Figure 1.5 - Chemical structure of PTFE (Polymers database, Polymers 2013 Copyright)

1.5. Scanning electronic microscopy (SEM)

An SEM micrograph is obtained by scanning a focused electron beam over an electrically conductive sample in vacuum. The interactions of these so-called primary electrons with the sample result in the generation of emitted electrons and photons that can be collected by appropriate detectors to give information on the composition and topography of the sample surface (C. Chen et al. 2007).

SEM (FEI XL 30 SFEG) was applied to analyse the surface morphology PVDF, PTFE, $PVDF^{f}$-TiO_2 and $PTFE^{f}$-TiO_2.

1.6. Fixed - bed Adsorption column

The specific mechanisms of adsorption in batch and continuous time systems rely on the diffusive characteristics of the solution and the adsorbent. Although macro transport is responsible for movement through the bed length, micro transport actually controls sorption by movement through the pores of the adsorbent (Hristovski et al., 2007).

The advantages of a fixed bed system include little operator attention, few concentration fines, easy inspection and cleaning for regeneration of adsorbent, and fewer instances of adsorbent particles in the effluent (Hristovski et al., 2007);(Peng et al., 2012).

Disadvantages include the large physical area needed to operate the fixed bed and the higher capital investment (Gürboğa & Tel, 2005).

For the purposes of this research, the fixed bed column was the design chosen.

The adsorption column, or contactor, removes impurities in the feed stream provided there is sufficient contact time between the impurity and the adsorbent (Gupta et al., 2009).

However, the end of the adsorption process is determined by the degree of high purification achieved and depends on the saturation of the adsorbent, the cost, and the environmental evaluation of purity (Uyguner et al., 2011).

The purity of a substance is monitored using a breakthrough curve, which estimates the time required before the sorptive capacity of the sorbent bed is reached, i.e. the bed life of an adsorbent (He et al. 2010).

The actual breakthrough curve appears after the breakpoint has been reached and monitors how quickly the exit concentration increases to the feed concentration, indicating little adsorption because the adsorption bed is at equilibrium with the feed concentration. An ideal breakthrough curve, the S-shape, is shown in Figure 1.6. The most important aspect of the breakthrough curve, as idealized in Figure 1.6, is the shape of the breakthrough because it determines the operating life-span of the adsorbent bed and the regeneration time needed for the bed length (He et al., 2010);(Mascolo et al., 2007);(Yu et al., 2012).

The shape of the breakthrough curve is dependent on several parameters, including the feed concentration, the feed flow rate, the size, shape, and type of adsorbent, and the temperature or pressure of the system (Mascolo et al., 2007);(Yu et al., 2012).

1.6.1. Analysis of column data

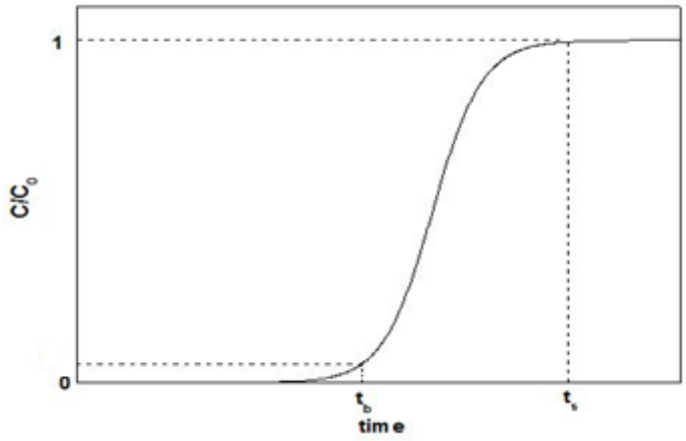

Figure 1.6 – Example of a breakthrough curve (Qi &Schideman, 2008)

From the breaktrough curves it is possible to calculate the breakthrough and saturation times (t_b and t_s respectively). The breakthrough time indicates the instant in which the adsorbate is effectively discharged on eluate, and the saturation time corresponds to the instant of adsorbate saturation point. The variation between the breakthrough and saturation times depends on the capacity of the column toward the quantity of applied adsorbate. A more efficient adsorption performance will be obtained as greater is the curve slope, i.e. as smaller is the gap between the breakthrough and saturation times (Qi & Schideman, 2008).
The uptake capacity (Qe) of the adsorbent can be calculated by equation 1.12 (Gürboğa and Tel 2005); (Hristovski, et al., 2007):

$$\mathbf{Qe = m_{ad}/M} \qquad \textit{Equation 1.12}$$

Where Qe is the HA uptake capacity, m_{ad} is the mass adsorbed (mg) and M is the adsorbent mass (g) (Hristovski, et al., 2007); (Gürboğa and Tel 2005).

The total amount of adsorbate (m_{total} (g)) sent through the column is calculated by equation 1.13 (Hristovski, et al., 2007); (Gürboğa and Tel 2005)

$$\mathbf{m_{total} = (C_0 \,.\, F \,.\, t_s) /1000} \qquad \textit{Equation1.13}$$

Where C_0 is the inlet concentration of adsorbate (mg/L), F is the flow of adsorbate (mL/min) and t_s is the saturation time (minutes) (Hristovski, et al., 2007);(Gürboğa and Tel 2005). The total removal percent of adsorbate (column performance) is calculated by equation 1.14 (Hristovski, et al., 2007);(Gürboğa and Tel 2005):

$$\mathbf{Total\ removal\ (\%) = (m_{ad}/m_{total}) \,.\, 100\%} \qquad \textit{Equation 1.14}$$

2. Aims of the present work

The main aims of this project are:

- To immobilize TiO_2 into fluoropolymers (PVDF and PTFE) pellets by photocatalysis;
- To optimize the preparation conditions to obtained maximum surface coverage;
- To investigate the photodegradation capacity and immobilization stability characteristics of the media;
- To investigate the adsorption capacity and stability of the media for humic acid;
- Develop a lab scale fixed bed adsorption column to assess the performance of the media;

3. Materials and Methods

3.1. Materials

3.1.1. Polymers

- Polymers PVDF and PTFE were purchased in Sigma-Aldrich;

3.2.2. Chemicals reagents

- Buffer solutions (pH 1, 3, 5, 7 and 10), Methylene Blue and Humic Acid AnalaR grade were Fisher Scientific, UK, reagents and used as received;
- TiO_2 P25 (anastase to rutile ratio between 70:30 and 80:20) by Degussa AEROXIDE®;

3.2.3. Instrumentation

- UV collimated beam reactor (Figure 3.1) design by Cranfield University, UK. The reactor consists of a collimated beam UV light, an UV irradiation controller time and a bottle of compressed air. The reactor has the following characteristics:

a) Dimension: 915 mm X 610 mm

b) Thickness: 3,0 mm

c) Intensity (I= 26 W/m^2)

d) UVC light (280-100 nm)

e) Irradiation time = 2 hours

a) b)

Figure 3.1 – Collimated beam UV light reactor a) and associated controller b)

- Scanning Electron Microscope – Philips/ FEI SFEG XL30 SEM, UK; (Figure 2.2)

The magnification was chosen between 1000 and 70 000 , the accelerating voltage was set to 20.0 kV and the working distance was in the range of 5.0–8.0mm. The resolution for this SEM instrument is 1.7 nm at 1 kV. Equipped with: standard Everhart-Thornley secondary-electron (SE) detector; ultra-high resolution (UHR) lens and in-lens SE detector; 4 quadrant backscattered electron (BSE) detector;

Figure 3.2 –Scanning electron microscope (SEM) – Philips/FEI XL 30 SFEG

- Spectrophotometer UV-V Jenway 6715, Bibby Scientific Limited (Group HQ), UK.
- Stir CB 161 shaker, Stuart®, UK.
- Pump Watson Marlow, model 520S, UK
- Plastic column, tubes and fittings purchased at Cranfield University;
- Philips & Bird Jar test equipment;
- Millex GP Filter 0.22 µm;

3.2. Methods

This work was performed at the Cranfield Water Institute, UK, from 12/09/12 to 26/06/13 and is divided into three distinct phases: Media preparation; Media performance and Adsorption Experiments.

3.2.1. Media preparation

3.2.1.1. Photocatalytic surface functionalization deposition (PSFD) of TiO_2 into PVDF and PTFE

Modification of the method described by Mazille, et al., 2009 a, as follows:

PVDF and PTFE pellets were washed with a solution of ethanol and water (1:1, v/v) to remove impurities.

TiO_2 solutions were prepared (Degussa P25) with different concentrations 0.5, 1.5 and 2.5 g / L at different pH values (1, 3, 5, 7 and 10).

Then PTFE or PVDF was added to a Petri dish and TiO_2 solutions to a thickness of 6 mm to allow the penetration of UV light. Different UV light distances were used, 230 mm and 100 mm.

The Petri dishes were inserted into the UV collimated beam reactor for 2 hours with magnetic stirring.

Scanning Electron Microscope – Philips/ FEI SFEG XL30 SEM, UK (figure 3.2) was used to evaluate fluoropolymers surface morphology.

3.2.2. Media performance

3.2.2.1. Evaluation of the photocatalytic activity of $PVDF^{f}$-TiO_2

In a Petri dish with $PVDF^{f}$-TiO_2 (3.0 g) prepared in different solutions of TiO_2 was added 30 mL of methylene blue (MB) with a concentration of 1 mg/L (figure 3.3). Petri dish was inserted in the collimated beam for 70 minutes. Aliquots of 1 mL were taken to evaluate photodegradation over time and MB was monitored by detecting UV absorbance intensity at 660 nm with Spectrophotometer UV-V Jenway 6715, Bibby Scientific Limited (Group HQ), UK. This test was done in triplicate.

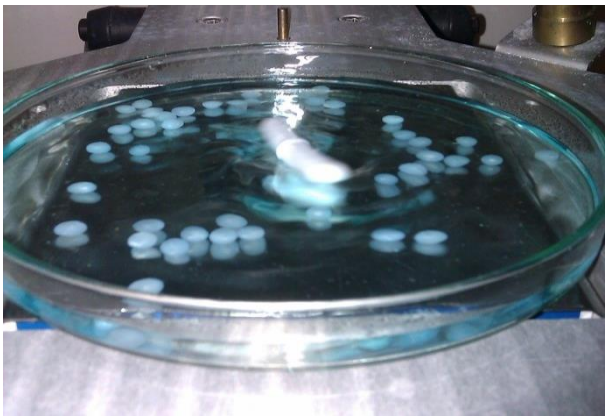

Figure 3.3–Photodegradation of Methylene Blue

3.2.2.2. Evaluation of photocatalytic stability after centrifugations in Jar test apparatus

Photocatalytic surface functionalization deposition (PSFD) of PVDF with a 1.5 g/L TiO_2 solution at pH 3 ($PVDF^{f}$-TiO_2) was prepared in the collimated beam.

Then the media $PVDF^{f}$-TiO_2 was submitted to 300 rpm centrifugations for 10 minutes in Philip & Bird Jar test equipment. Then $PVDF^{f}$-TiO_2 was further evaluated according to the photocatalytic capacity to degrade methylene blue (1 mg/L) during 70 minutes. The experiment was performed in triplicate and Scanning Electron Microscope – Philips/ FEI SFEG XL30 SEM, UK was used to evaluate the surface morphology.

3.2.2.3. Blanks

Different blanks were performed:

a) PVDF and MB (1 mg/L) expose to UV light, for 70 minutes.

b) PVDF and MB (1 mg/L) in the dark, for 70 minutes.

c) PVDF[f]- TiO_2 (1.5g/L pH 3) and MB (1 mg/L) in the dark, for 70 minutes;

d) (PVDF + TiO_2 1.5 g/L pH =3) prepared in the dark. Following three centrifugations in a stirrer Jar test apparatus in between photodegradation of methylene blue.

3.2.3. Adsorption experiments

Adsorption experiments were based OECD Guidelines for testing of chemicals, Test No. 106: Adsorption – Desorption using a batch equilibrium Method

3.2.3.1. Adsorption isotherm of HA on TiO_2 powder

3.2.3.1.1. Calibration curve

From a stock solution of humic acid (500 mg/L) different solutions were prepared by dilution. A Spectrophotometer UV-V Jenway 6715, Bibby Scientific Limited (Group HQ), UK, was used to construct the calibration curve at wavelength of 254 nm. (Figure 8.1 – Annex I)

3.2.3.1.2. Adsorption of humic acid on TiO_2 powder

The affinity of HA to TiO_2 was determined by the batch equilibrium experiments performed in the dark. Research was carried out on a suspension, by mixing 100 mL of various HA concentrations (1.0; 2.0; 4.0; 8.0; 10.0; 15.0; 30.0; 40.0 and 50.0 mg/L) at pH 5 and a fixed amount of TiO_2 (0.02g). To determine the isotherm of adsorption, the solutions were kept in a Stir CB 161 shaker, Stuart®, UK, at 160 rpm and 20ºC. After 24 hours of the samples were removed and filtered using a Millex-GP Filter Unit 0.22 μm. The concentrations were measured by Spectrophotometer UV-V Jenway 6715, Bibby Scientific Limited (Group HQ), UK, at 254 nm.

3.2.3.2. Adsorption isotherm of HA on PVDF^{f}-TiO_2

The affinity of HA to PVDF^{f}-TiO_2 was determined by the batch equilibrium experiments performed in the dark. Research was carried out on a suspension by mixing 50 mL of various HA concentrations (0.5; 1.0; 2.0; 4.0; 8.0; 10.0; 12.0 and 20.0 mg/L) at pH 5 and a fixed amount of PVDF^{f}-TiO_2 (10.0g). To determine the isotherm of adsorption, the solutions were kept in a Stir CB 161 shaker, Stuart®, UK, at 160 rpm and 20ºC. After 24 hours of the samples were removed and filtered using a Millex-GP Filter Unit 0.22 μm. The concentrations were measured by Spectrophotometer UV-V Jenway 6715, Bibby Scientific Limited (Group HQ), UK, at 254 nm.

3.2.3.3. Photocatalytic degradation of humic acid using PVDF^{f}-TiO_2 – Regeneration time

Humic acid with a concentration of 5mg/L was added to a Petri dish with PVDF^{f}-TiO_2. The petri dish was inserted in the collimated beam for 250 minutes. Aliquots of 1mL were taken to evaluate photo degradation over time and the equilibrium absorbance determined by Spectrophotometer UV-V Jenway 6715, Bibby Scientific Limited (Group HQ), UK, at 254 nm. This test was performed in triplicate.

3.2.3.4. Adsorption stability/Regeneration of PVDF^{f}-TiO_2

3.2.3.4.1. Adsorption/ regeneration cicles

The process described in 3.2.3.2 was repeated eight times with a regeneration of 2 hours using the UV reactor.

Adsorption isotherms after 8 adsorption/ regeneration cycles were plotted to evaluate adsorption stability

3.2.3.5. Blanks

Different adsorption blanks were performed to evaluate the adsorption capacity of PVDF and 0.22 μm filter units:

a) Humic acid adsorption on PVDF;
b) Filtration humic acid samples at different concentrations through the filter 0.22μm.

Aliquots of 1mL were taken to evaluate photodegradation over time and a Spectrophotometer UV-V Jenway 6715, Bibby Scientific Limited (Group HQ), UK, was used to determine the equilibrium absorbance. This test was performed in triplicate.

3.2.3.6. Fixed- bed adsorption column

An adsorption column was developed in order to evaluate the new media ($PVDF^f$-TiO_2) for further application in industry.

$PVDF^f$-TiO_2 (mass =1000 g) was packed into a transparent plastic column of 7 cm inner diameter and 30 cm of height, corresponding to a bed volume of 654.24 cm^3 (Figure 3.4).

In order to evaluate the adsorption capacity, a solution of HA (5 mg/L) was allowed to percolate through the column from the bottom (up stream flow) at flow rates of 10.4; 5.19; 3.25; 2.60 and 1.30 mL/min, using a Watson Marlow 520S pump, UK (Figure 3.5).

Samples were collected from the exit of the bed column at 10 minutes time intervals and analyzed for HA using a Spectrophotometer UV-V Jenway 6715, Bibby Scientific Limited (Group HQ), UK, to determine the equilibrium absorbance at a wavelength of maximum absorbance of 254 nm. Operation of the column was stopped when the effluent HA concentration exceeded 99.5% of its initial concentration

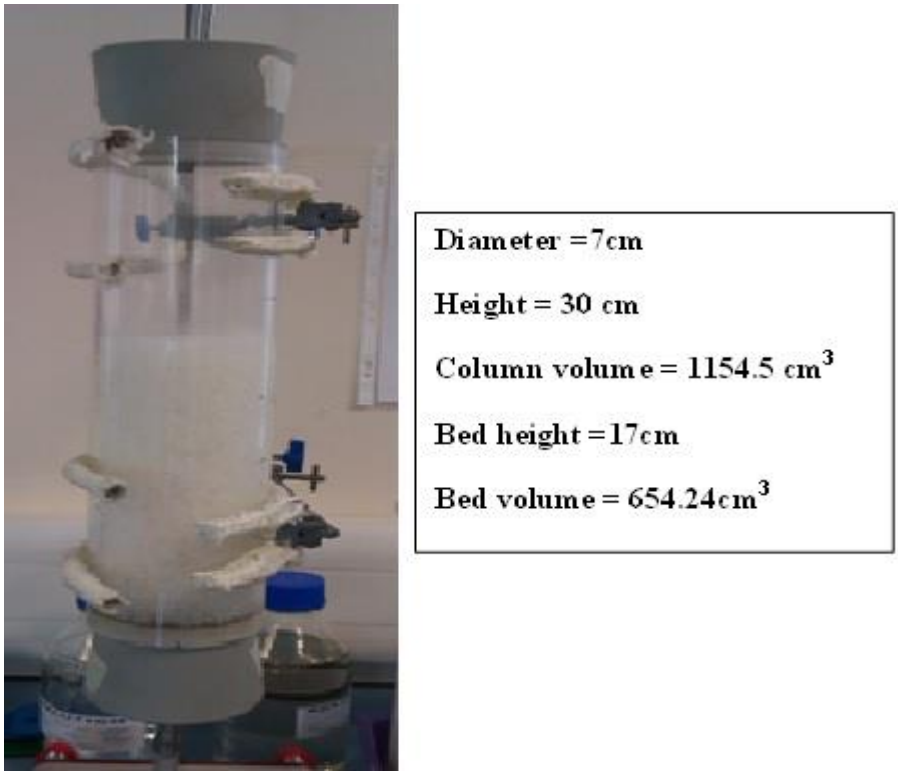

Figure 3.4 – Fixed-bed adsorption column

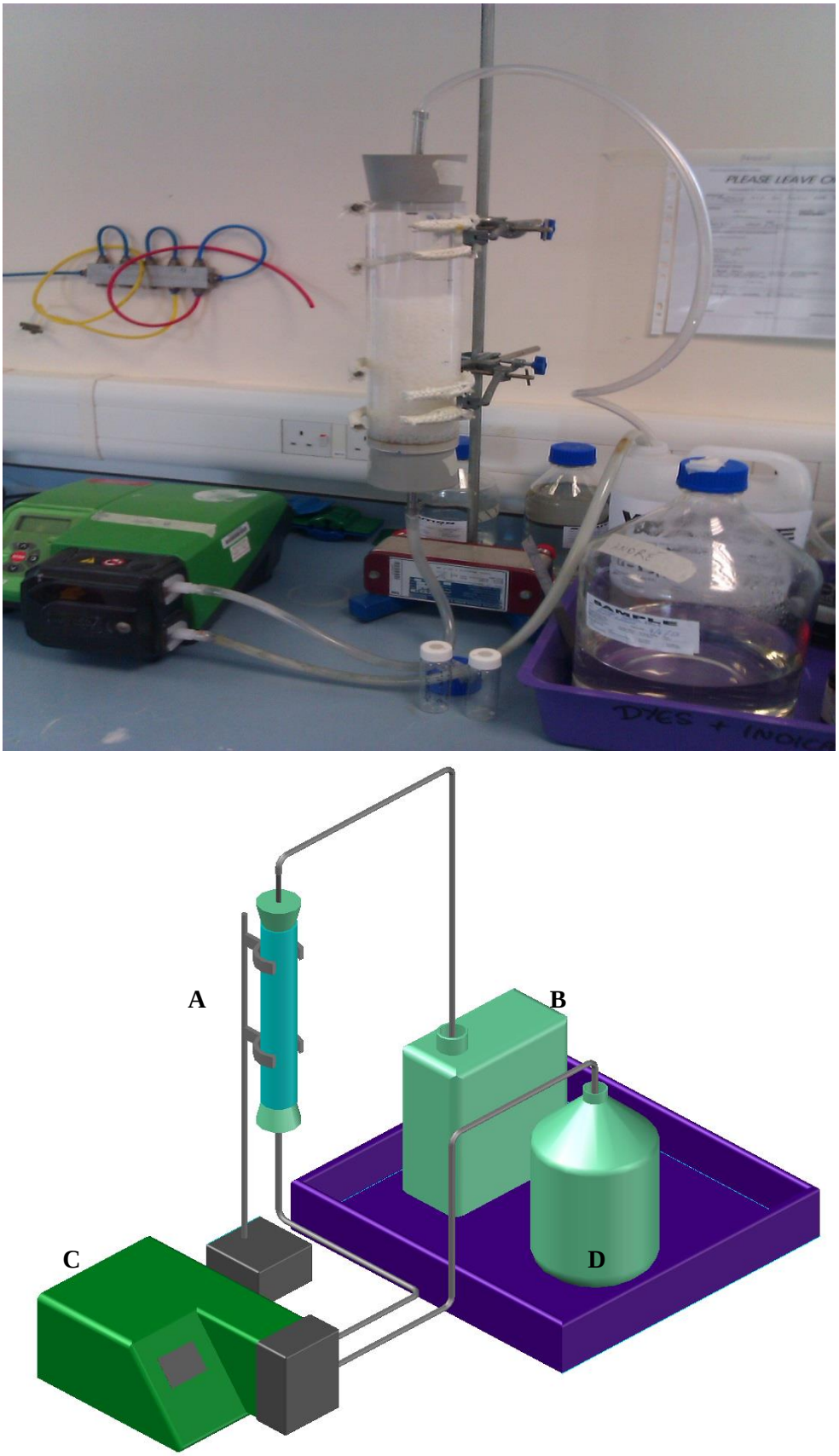

Figure 3.5 – Schematic overview of the adsorption column – A) Fixed-bed adsorption column B) Outlet container C) Watson Marlow 520S pump, UK D) Inlet container (Feed concentration of HA = 5 mg/L)

4. Results and discussion

4.1 Media preparation

4.1.1. Observation of PVDF and PTFE surfaces under SEM

The figures 4.1 and 4.2 show the SEM micrograph of the fluoropolymers surface before the polymer surface functionalization deposition of TiO_2. The surfaces are both predominately smooth, with a spherical shape.

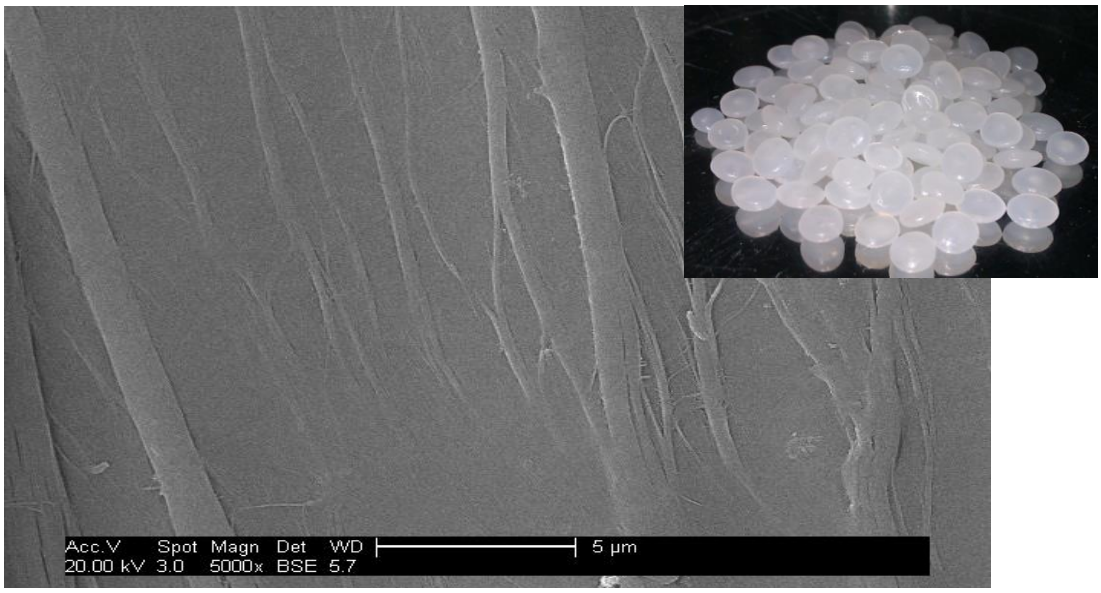

Figure 4.1 –PVDF surface (x5000)

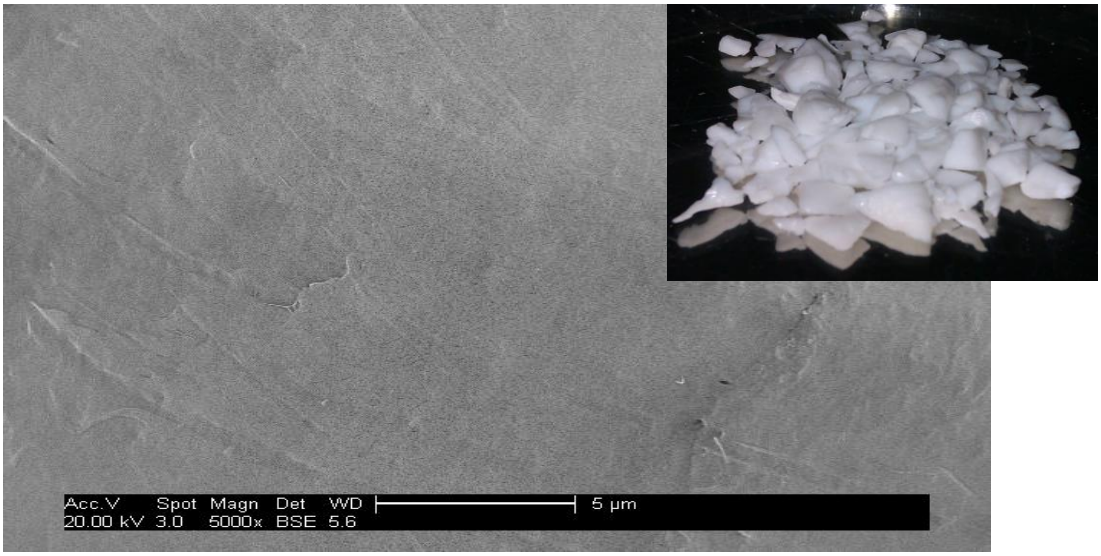

Figure 4.2 –PTFE surface(x5000)

4.1.2. Photocatalytic surface functionalization deposition of TiO_2 into PVDF and PTFE surfaces

After a TiO_2 PSFD treatment at pH 3, the aggregated TiO_2 nanoparticles cover significantly the surface of PVDF (figure 4.3) when compare to PTFE (figure 4.4). The main reason for such coverage, might be the chemical structure of the polymers, explained by the mechanistic suggestion for TiO_2 photocatalytic surface functionalization deposition as a function of pH shown figure 4.13

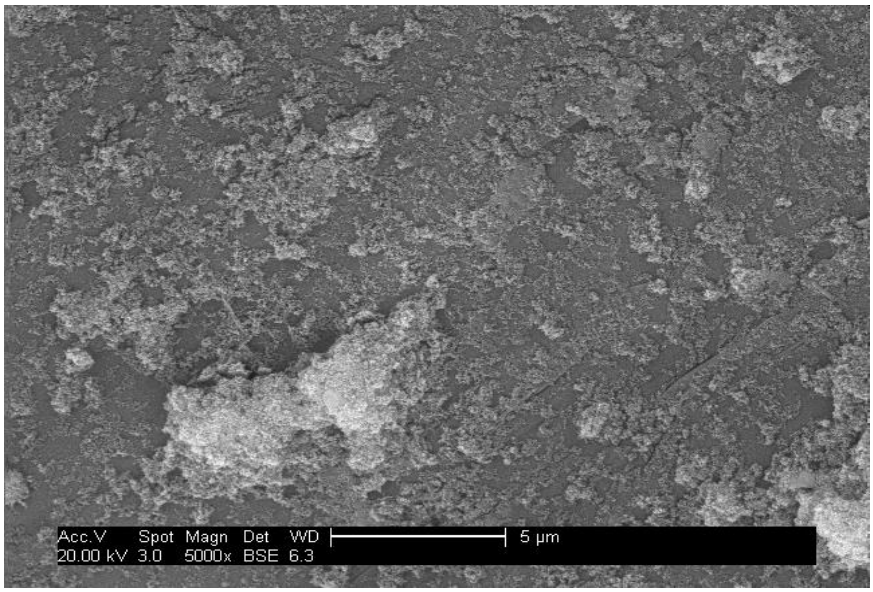

Figure 4.3 –Scanning electron microscopic image of PVDF^f-TiO_2 prepared with a 1.5 g/L TiO_2 solution at pH 3 (UV time = 2h, light distance= 100mm) (x5000)

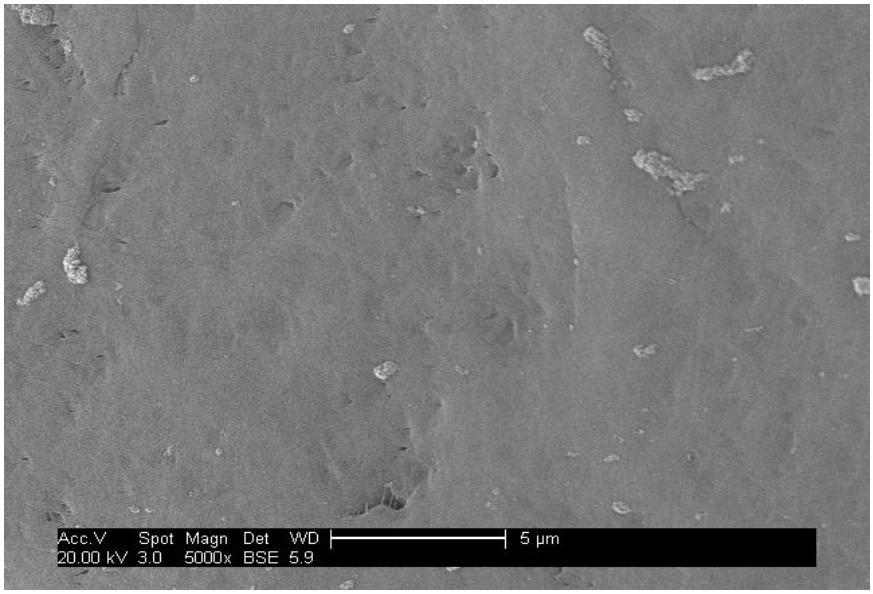

Figure 4.4 - Scanning electron microscopic image of PTFE^f-TiO_2 prepared with a 1.5 g/L TiO_2 solution at pH 3 (UV time = 2h, light distance = 100 mm) (x5000)

Mazille et al.,(2009 a) (figure 4.5) obtained similar results for TiO_2 PSFD treatment at pH 5 to cover PVF.

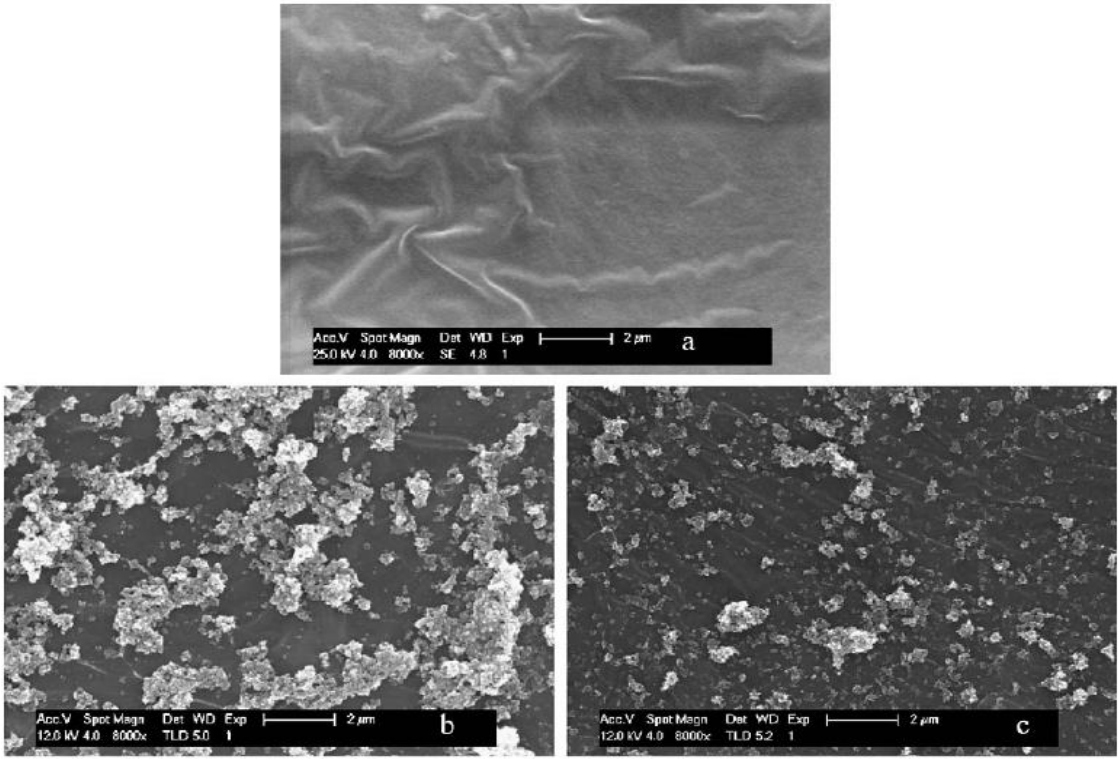

Figure 4.5 - Scanning electron microscopic images of a) PVF b) PVF^f-TiO_2 prepared at pH 5 (external side) and c) PVF^f-TiO_2 prepared at pH 5 (internal side) (Mazille et al., 2009, a)

According to the scanning electron microscopic images, the fluoropolymer PVDF shows a better ability for the photocatalytic functionalization surface deposition of TiO_2 when compared with PTFE. PVDF was therefore chosen for further experimental work.

4.1.3. Influence of UV light distance (100 mm e 230 mm)

After the evaluation of different distances from UV light beam, the distance 100 mm (figure 4.6) shows significant coverage of PVDF surface compare with the distance 230 mm (figure 4.7). Therefore the distance 100 mm was used as a fixed parameter in further experimental work.

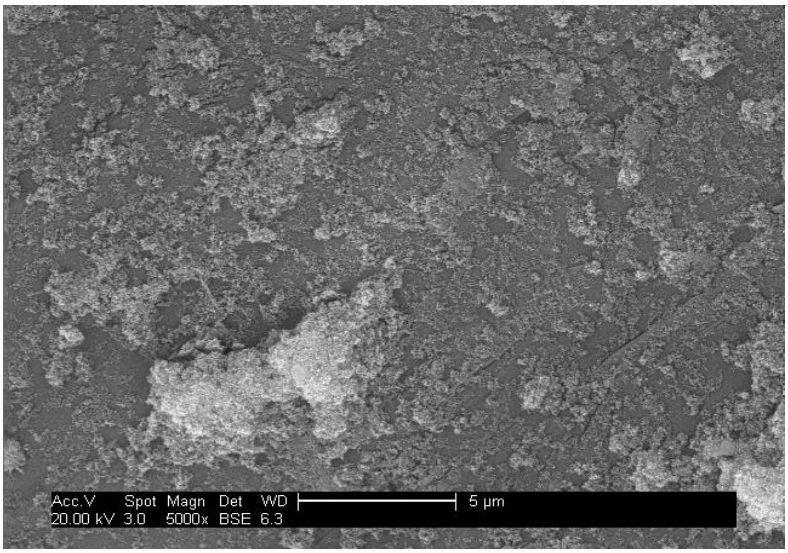

Figure 4.6 - Scanning electron microscopic image of PVDF^f-TiO_2 prepared with a 1.5 g/L TiO_2 solution at pH 3 (UV time = 2h, light distance= 100 mm) (x5000)

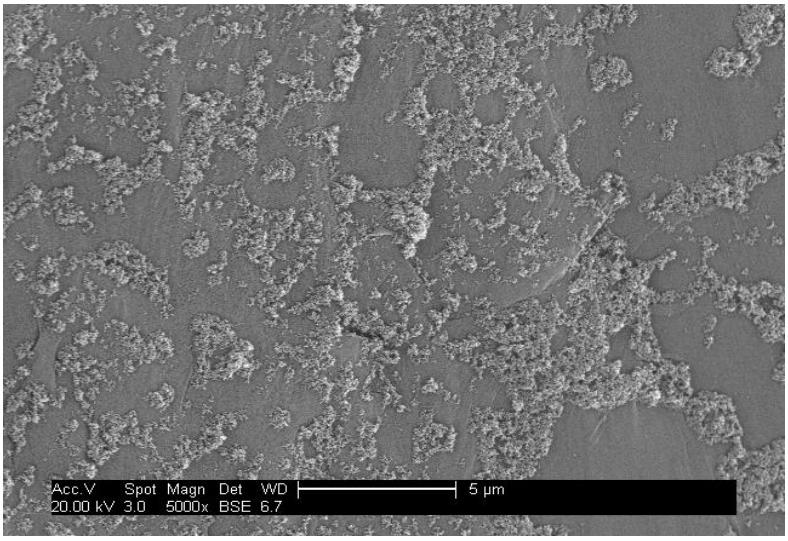

Figure 4.7- Scanning electron microscopic images of PVDF^f-TiO_2 prepared with a 1.5 g/L TiO_2 solution at pH 3 (UV time = 2h, light distance= 230 mm) (x5000)

4.1.4. Scanning electron microscopic images of $PVDF^f$-TiO_2 at different pH

The following results shows the PVDF surface after functionalization surface deposition with different pH solutions of TiO_2 (1.5 g/L) (2h UV d=100 mm).

According to the experimental results, (figures 4.8; 4.9; 4.10; 4.11; 4.12) there is a decrease surface coverage at higher pH. When submitting PVDF to a TiO_2 PSFD treatment, the immobilization of the TiO_2 assisted by polymer surface functionalization occurs. Thus, after the treatment performed at pH 3 (figure 4.9), the polymer is fully covered with TiO_2, whereas after the treatment at pH 10 (figure 4.12), TiO_2 was hardly detected. These results show that it is possible to control the extent of TiO_2 deposition by varying the pH.

Under acidic conditons, (figures 4.8 (pH 1) and 4.9 (pH 3)) there is a minimal difference in surface coverage, with an optimal coverage apparent at pH 3.

However at neutral and basic pH there is significantly less coverage due the mechanism suggested in figure 4.13.

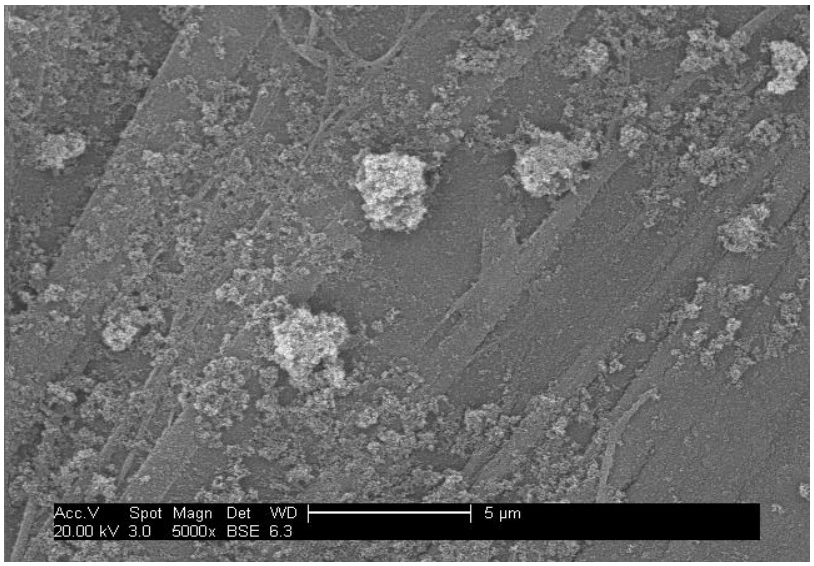

Figure 4.8 –PVDF surface after PSFD with TiO_2 (1.5 g / L at pH =1 solution) (x5000)

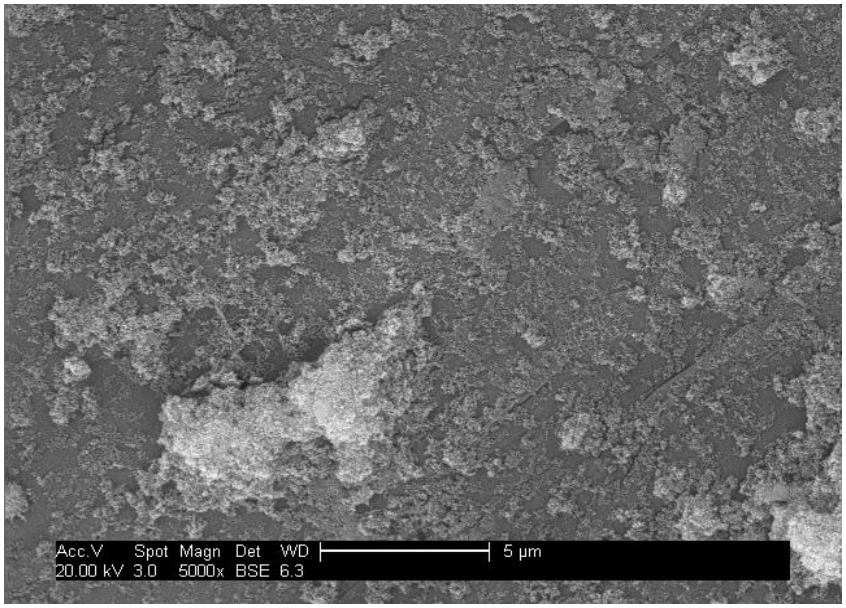

Figure 4.9 – PVDF surface after PSFD with TiO_2 (1.5 g / L at pH =3 solution) (x5000)

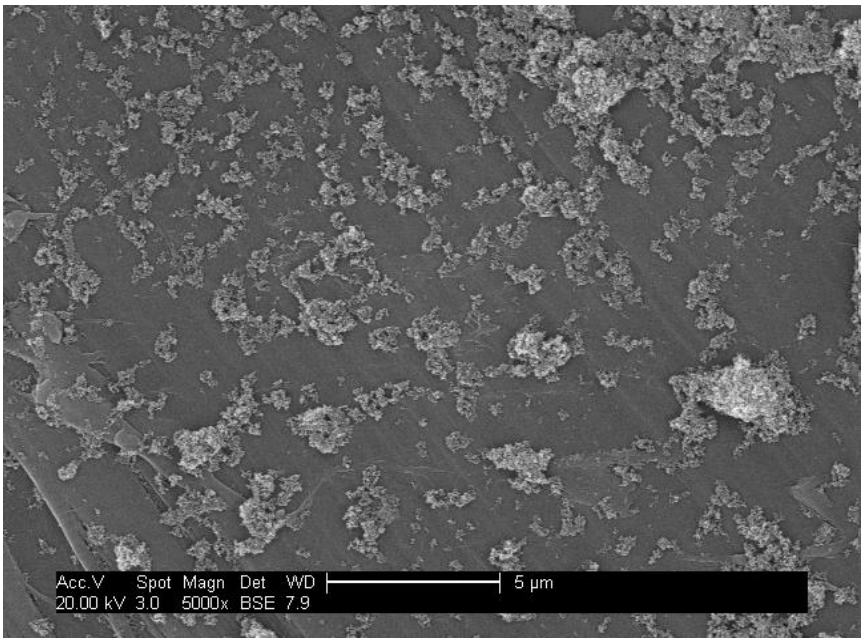

Figure 4.10– PVDF surface after PFSD with TiO_2 (1.5 g / L at pH =5 solution) (x5000)

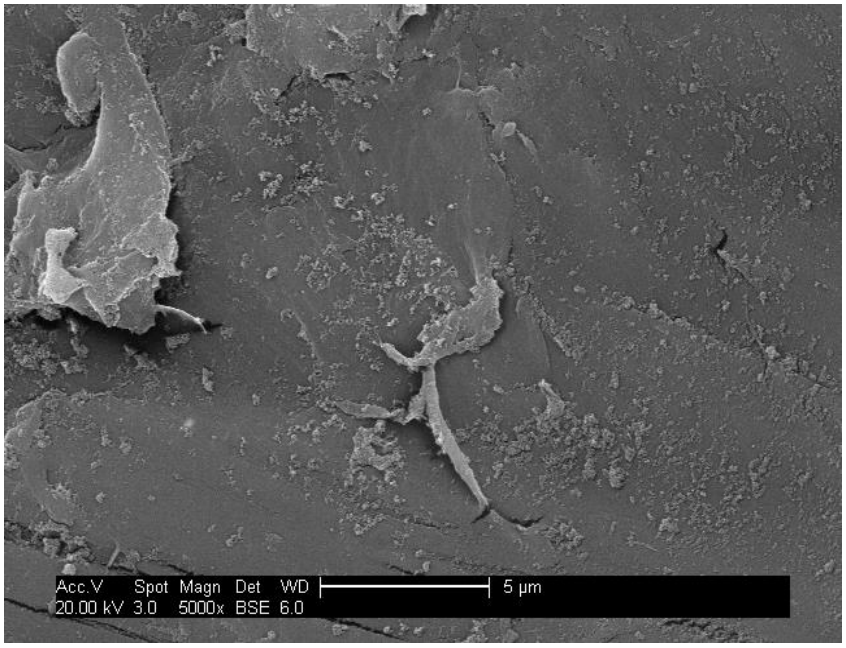

Figure 4.11 – PVDF surface after PSFD with TiO_2 (1.5 g / L at pH =7 solution) (x5000)

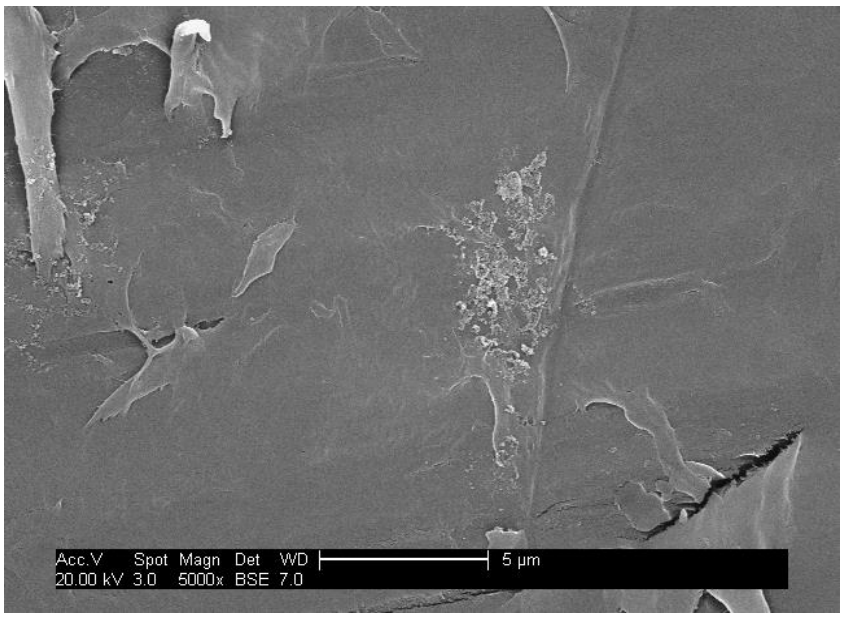

Figure 4.12 – PVDF surface after PSFD with TiO_2 (1.5 g / L at pH =10 solution) (x5000)

Mazille et al.,(2009 a) refer that under irradiation in aqueous TiO_2 suspension in equilibrium with air, PVF films suffer photocatalytic attacks leading to C=O, COOH groups and to the elimination of fluorine. When the pH of the aqueous solution is acidic the polymer surface is negatively charged since the TiO_2 PSFD treatment induced the formation of functional groups like COO^- and the superficial charge of TiO_2 P25 is positive (its isoelectric point is near to 7). Consequently an electrostatic attraction binds the TiO_2 nano particles to the

polymer surface (Figure 4.13). The mechanism suggested by Mazille et al, (2009 a) was considered to explain the binding mechanism of TiO_2 nanoparticles onto PVDF surface.

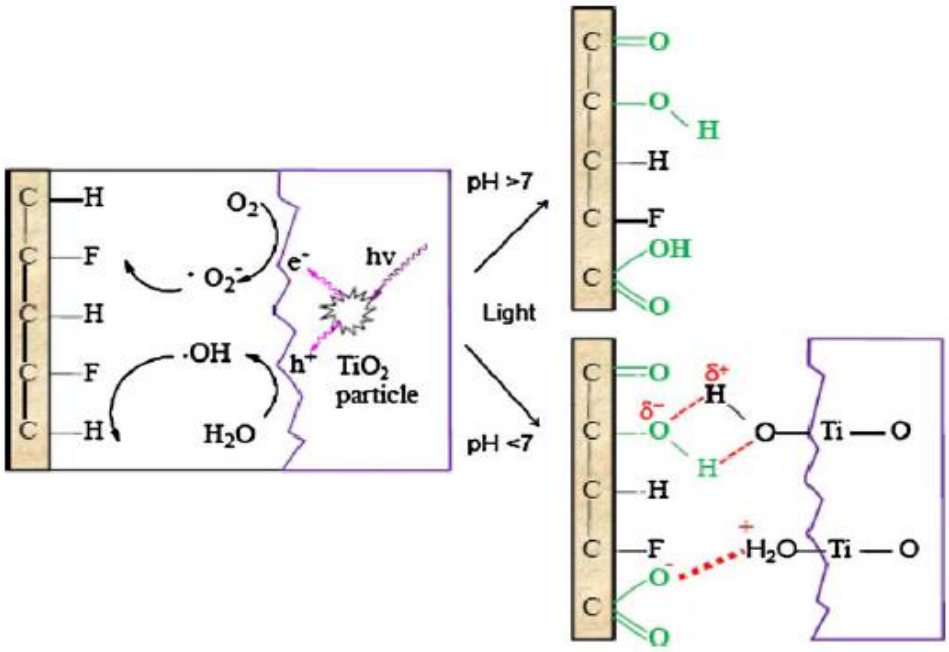

Figure 4.13 – Mechanistic suggestion for TiO_2 photocatalytic surface functionalization-deposition as a function of pH (Mazille, et al., 2009 a)

4.2. Media Performance

4.2.1. Photodegradation of methylene blue using PVDF^f - TiO_2 prepared at different concentrations and pH of TiO_2 solutions

Methylene blue (MB) is a typical azo dye. It can be efficiently degraded by TiO_2 nanoparticles and the concentration of MB in solution is easily detected by UV-vis spectroscopy (Hwang et al., 2012) (Kuo & Ho, 2001).

The PVDF^f-TiO_2 prepared at different pH and concentration of TiO_2 solutions was used to obtain kinetic data for degradation of aqueous solution of MB dye in the photo-reactor. The aims were to analyze kinetic data and obtain kinetic parameters, to determine the optimum TiO_2 concentration and pH conditions to prepare the media for further adsorption studies of humic acid.

The photodegradation of MB ($C_{16}H_{18}N_3SCl$) in the presence of UV light and oxygen occurred over the TiO_2 photocatalyst surface (Carvalho et al., 2010) (Chang et al., 2004)(Shimizu et al., 2007).

Houas et al., (2001) reported that the reaction mechanism for the photocatalytic degradation of methylene blue over TiO_2 catalyst is treated as heterogeneous reaction following a Langmuir-Hinshelwood mechanism. It consists of three steps which are described by equations 4.1 to 4.3:

1) Adsorption:

$C_{16}H_{18}N_3SCl + S^\circ \leftrightarrow C_{16}H_{18}N_3SCl\bullet S^\circ$ ***Equation 4.1***

$O_2 + S^\circ \leftrightarrow O_2 \bullet S^\circ$

2) Surface reaction (MB mineralization)

$C_{16}H_{18}N_3SCl\bullet S^\circ + 25.5\ O_2 \bullet S^\circ \leftrightarrow 16CO_2\bullet S^\circ + 6H_2O\bullet S^\circ + 3HNO_3\bullet S^\circ + H_2SO_4\bullet S^\circ + HCl\bullet S^\circ$ ***Equation 4.2***

3) Desorption

$CO_2\bullet S^\circ \leftrightarrow CO_2 + S^\circ$ ***Equation 4.3***

$H_2O\bullet S^\circ \leftrightarrow H_2O + S^\circ$

$HNO_3\bullet S^\circ \leftrightarrow HNO_3 + S^\circ$

$H_2SO_4\bullet S^\circ \leftrightarrow H_2SO_4 + S^\circ$

$HCl\bullet S^\circ \leftrightarrow HCl + S^\circ$

Where S° represents the active site on the catalyst surface.

The below graphs (Figure 4.14 to 4.17) shows the photodegradation of methylene blue by $PVDF^{f}$-TiO_2 prepared at different pH and concentrations.

The photocatalytic activity of TiO_2 in the degradation process is influenced by several parameters such as the phase composition, band-gap energy, surface area, particle size, crystallinity, electron-hole recombination rate and the existence of several dopants ions (Goetz et al., 2009); (Mascolo et al., 2007);(Ngang et al., 2012);(Prieto et al., 2005).

Effect of pH in the preparation of the $PVDF^{f}$-TiO_2 media

The disappearance of the colour of methylene blue as a function of the irradiation time followed an exponential decay. It was observed, Figure (4.14 to 4.16) that the degradation decay curve of methylene blue is higher in $PVDF^{f}$- TiO_2 prepared under acidic conditions, compared to the decay curve of methylene blue when $PVDF^{f}$-TiO_2 is prepared under pH 7 (Figure 4.17).

These results are interesting because they correlate well with the surface coverage of the media shown in figures 4.8 to 4.11. When the media is prepared under acidic conditions the photodegradation activity of $PVDF^{f}$-TiO_2 is higher, due to the higher surface coverage, when compared to the lower photodegradation activity of the media prepared under neutral and basic pH conditions (Table 4.1).

The $PVDF^{f}$-TiO_2 prepared with a TiO_2 solution 1.5g/L at pH 3 shows the photodegradation of 97.58% of methylene blue after 70 minutes (Figure 4.15 and Table 4.1).

Effect of concentration in the preparation of the $PVDF^{f}$-TiO_2 media

Figures 4.14 to 4.17 show the slight difference in photodegradation percentage of $PVDF^{f}$-TiO_2 prepared under different concentrations of TiO_2 solutions. Apparently there is no significant effect of the concentration of TiO_2 solutions on the preparation of $PVDF^{f}$-TiO_2.

These outcomes might be due the turbid appearance of TiO_2 solutions and the resulting effect on light penetration which is responsible for the activation of catalyst (Mazille, et al. 2009 a)(Páez et al. 2011)(J. Yu et al. 2006)(Zhang et al. 2008).

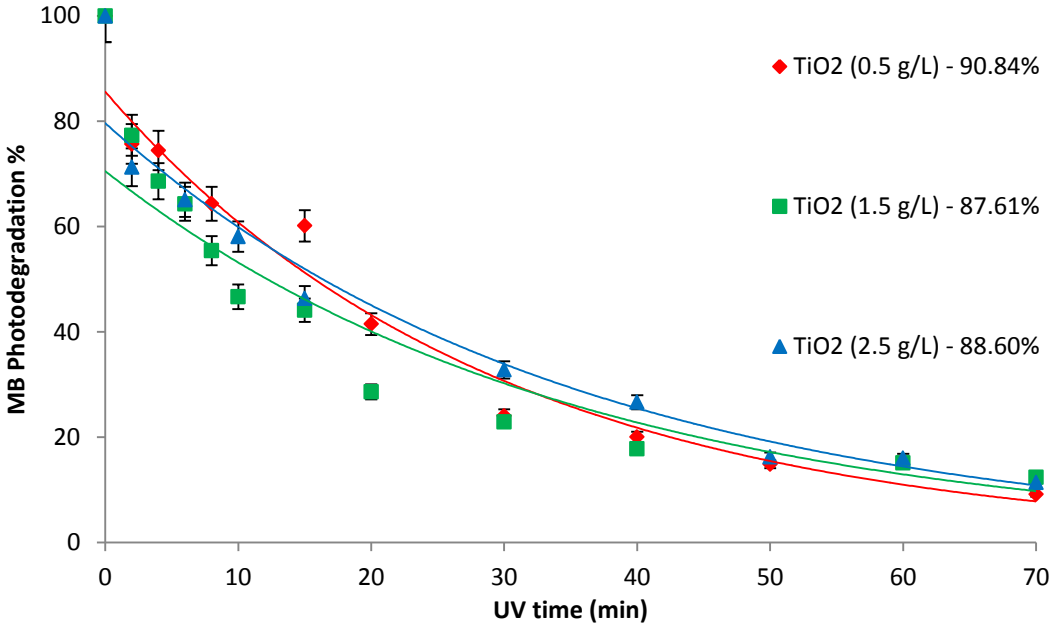

Figure 4.14 – Photodegradation of Methylene blue – PVDF^f- TiO_2 prepared at pH = 1

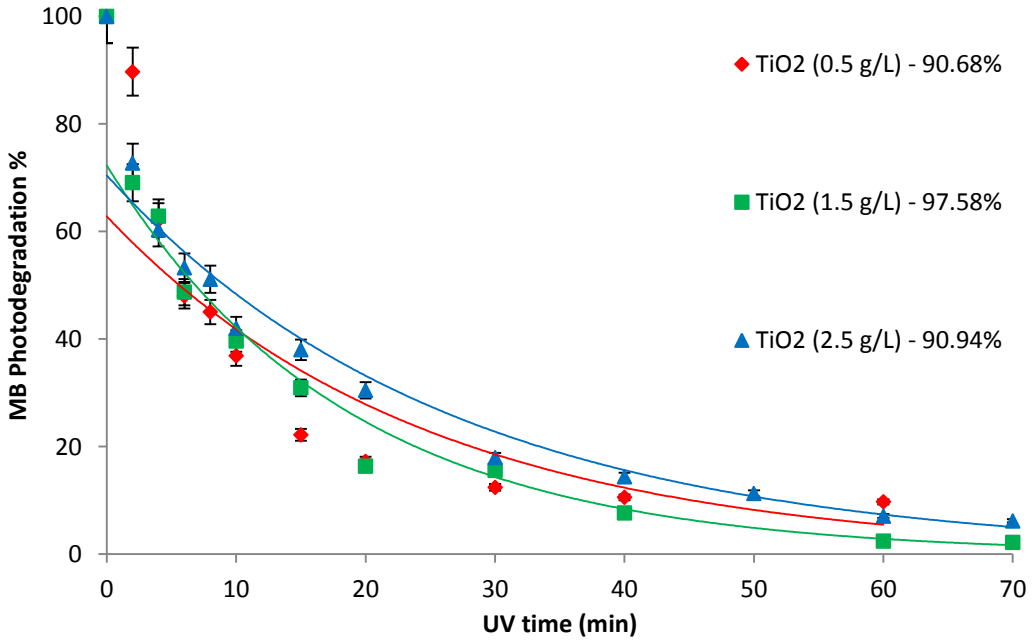

Figure 4.15 - Photodegradation of Methylene blue – PVDF^f- TiO_2 prepared at pH = 3

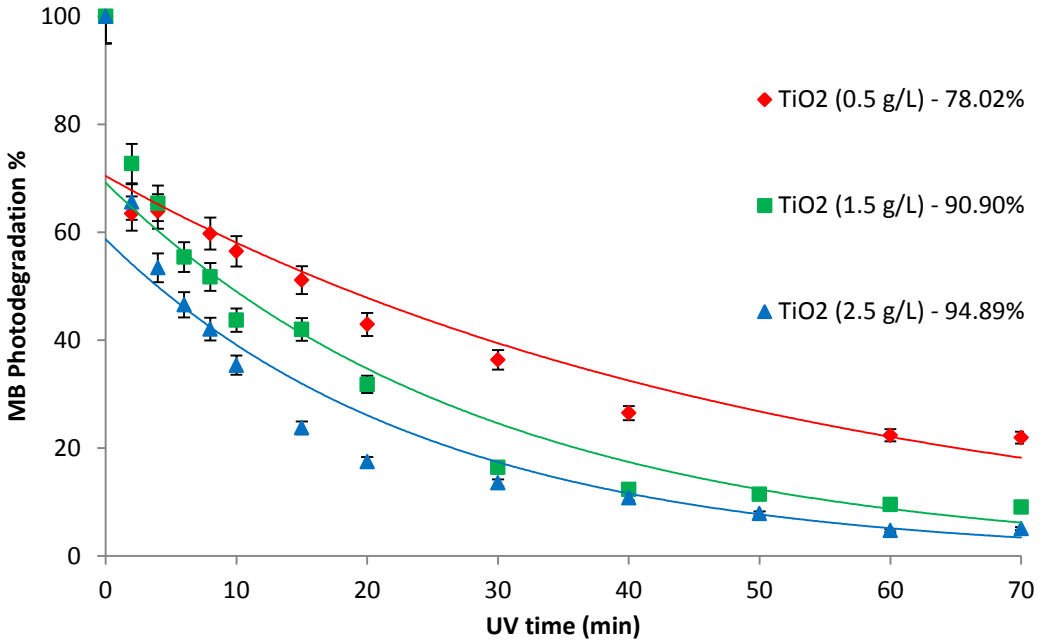

Figure 4.16 - Photodegradation of Methylene blue – PVDF^f- TiO_2 prepared at pH = 5

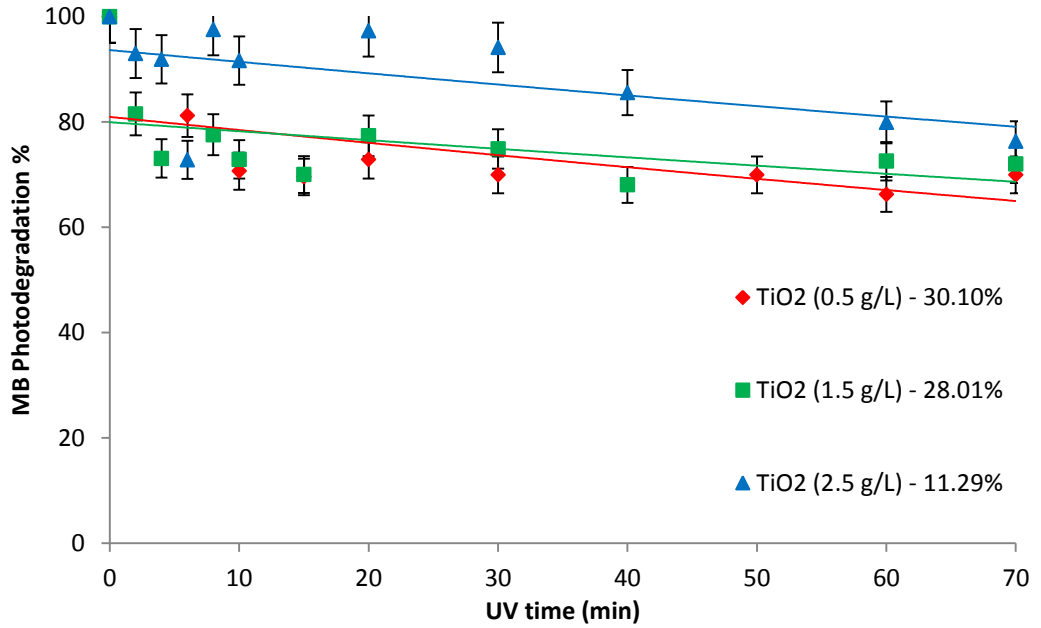

Figure 4.17– Photodegradation of Methylene blue – PVDF^f- TiO_2 prepared at pH = 7

Photodegradation kinetics

In general, the kinetics of photocatalytic degradation of organic pollutants on the semiconducting oxide has been established and can be described well by the apparent pseudo first order kinetics ln (Ci/C) = K_{app}.t, where K_{app} is the apparent rate constant, C_i is the initial concentration of MB and C is the concentration of MB at the time t (Bizani et al. 2006); (Banerjee, Dasgupta, and De 2007); (Y. Li et al. 2006); (Q. Li et al. 2011); (Páez et al. 2011).

Only the photodegradation kinetics lines for $PVDF^f$-TiO_2 prepared under acidic conditions (pH 1, 3 and 5) were plotted (Figures 4.18; 4.19 and 4.20) due the photocatalytic activity of the media.

Figures 4.18 to 4.20 show the linear relation of ln (Ci/C) versus irradiation time for the degradation of MB. Also, the determined apparent rate constants (K_{app}), linear regression coefficient (R^2), degradation efficiency of MB after irradiating for 70 minutes and half-life time for different conditions used to prepare $PVDF^f$-TiO_2 are presented in Table 4.1.

K_{app} and half-life time ($t_{1/2}$) were used as parameters to determine the best conditions (pH and concentration) to prepare the $PVDF^f$-TiO_2, assuming in those optimized conditions there is an increase of surface coverage of PVDF with TiO_2 nanoparticles.

The degradation rate of MB by $PVDF^f$-TiO_2 was higher when pH 3 was used to prepare the media, when compared with pH 1 and pH 5. According to results expressed in table 4.1, the $PVDF^f$-TiO_2 prepared with 1.5g/L at pH 3 shows a degradation of 97.58%. The Kapp and $t_{1/2}$ were calculated using the L-H equations (Equations 1.4 and 1.5) and the values are 0.0539 min^{-1} (R^2= 0.9757) and 12.86 min, respectively (the highest K_{app} and the lowest $t_{1/2}$ found during this comparison).

According to the obtained results, the optimum concentration and pH conditions to prepare $PVDF^f$-TiO_2 were considered to be a solution of 1.5 g/L of TiO_2 at pH 3.

As shown in Figure 4.20, $PVDF^f$-TiO_2 prepared with TiO_2 solutions at pH 5 (and indeed, at higher pH), shows an overall increase in K_{app} when the concentration of TiO_2 increases, with pseudo first order kinetics and a rate of 0.0206 min^{-1} to 0.0405 min^{-1}, compared with the results at pH 1. There is also a decrease of degradation half-life from 33.65 to 17.11, respectively.

Based on these results, it was concluded that is it possible to control the photocatalytic surface deposition functionalization of TiO_2 onto PVDF, which is supported by Mazille et al., 2009,a on PVF films.

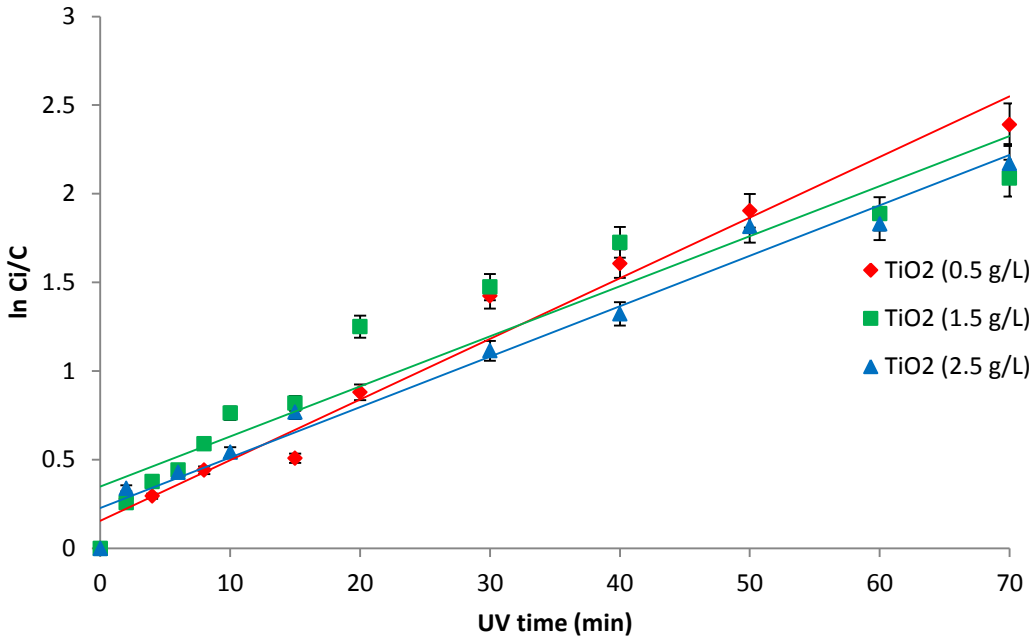

Figure 4.18 – Pseudo-first-order kinetics - PVDF^f-TiO$_2$ prepared at pH = 1

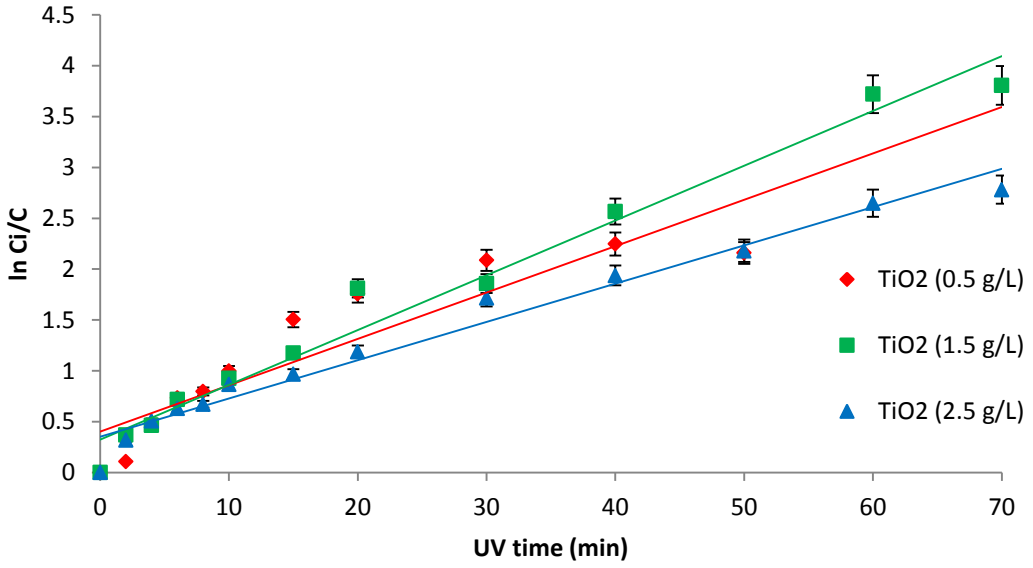

Figure 4.19 - Pseudo-first-order kinetics – PVDF^f-TiO$_2$ prepared at pH = 3

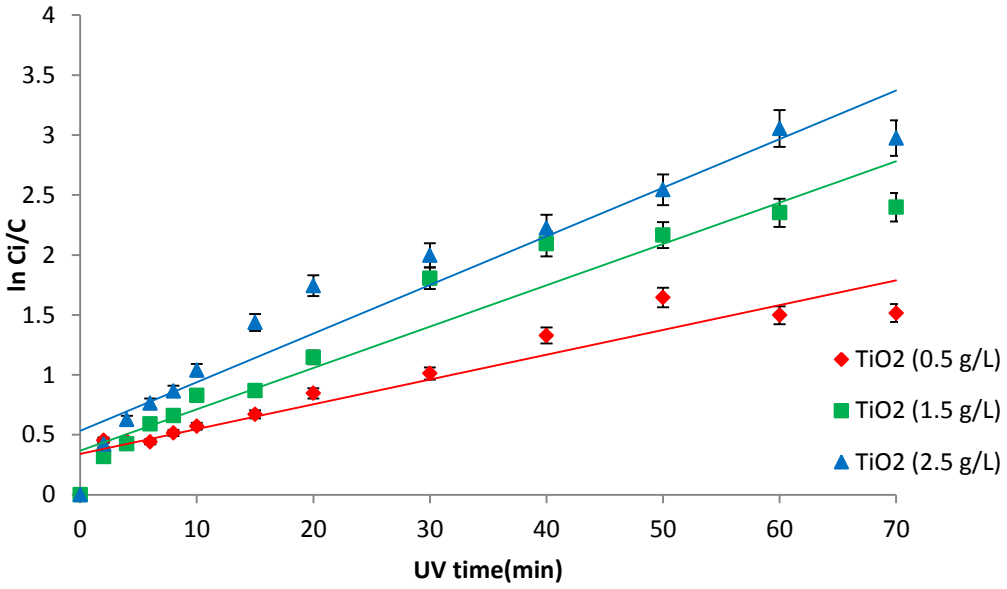

Figure 4.20- Pseudo-first-order kinetics – PVDF^f-TiO$_2$ prepared at pH = 5

Table 4.1 – Photodegradation of Methylene Blue (%) and Pseudo-first-order kinetics parameters

	pH	[TiO$_2$] g/L	% Methylene Blue Photodegradation	K_{app} (min^{-1})	R^2	t ½ (min)
PVDF^f – TiO$_2$	**1**	0.5	90.83	0.0342	0.9750	20.26
		1.5	87.61	0.0282	0.9037	24.57
		2.5	88.60	0.0285	0.9767	24.32
	3	0.5	90.68	0.0456	0.8388	15.19
		1.5	**97.58**	**0.0539**	**0.9718**	**12.85**
		2.5	90.94	0.0376	0.9718	18.43
	5	0.5	78.02	0.0206	0.9008	33.65
		1.5	90.90	0.0345	0.9280	20.09
		2.5	94.89	0.0405	0.9311	17.11

4.2.2. Evaluation of photocatalytic activity of PVDF^{f}-TiO_2 after centrifugations in Jar test apparatus

PVDF^{f}-TiO_2 prepared in optimum conditions (1.5 g/L of TiO_2 at pH 3) was centrifuged at 300 rpm for 10 minutes in a JAR test equipment to evaluate the physical strength of the bond between PVDF and TiO_2.

Right after the centrifugation the media PVDF^{f}-TiO_2 was evaluated regarding the photocatalytic activity to degrade methylene blue. This procedure was performed three times successively.

Figure 4.21 shows the photodegradation decay curve of MB. It is possible to observe the same decay shape curve, after submitted the media to three centrifugations. The objective of centrifugation was to submit the media to rotation conditions to remove TiO_2 nanoparticles from the surface and thus determine the stability and strength of the electrostatic attraction, propose by the mechanism in Mazille, et al., (2009 a).

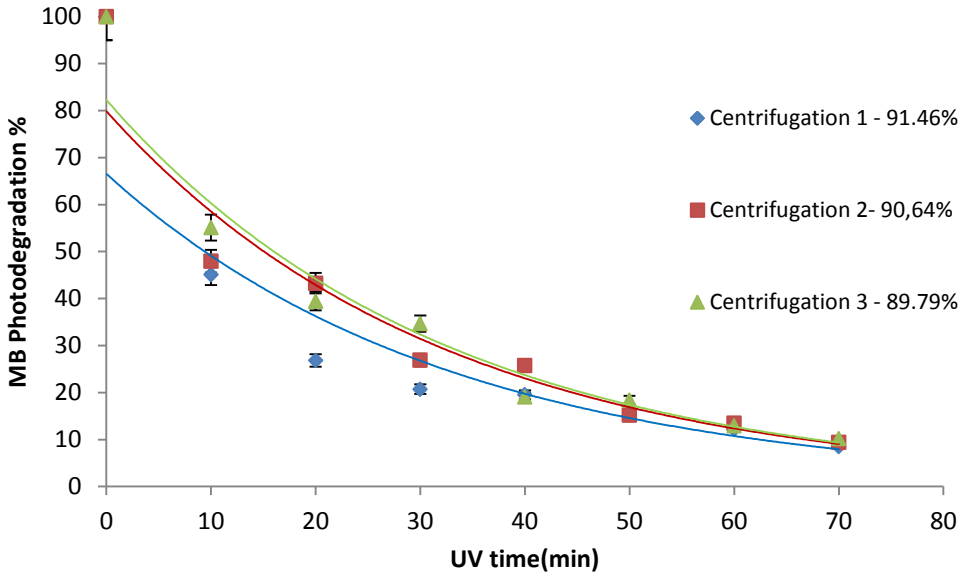

Figure 4.21 – Photodegradation of Methylene blue (PVDF^{f}- TiO_2 submitted to three centrifugations)

The SEM figure 4.22 at different magnifications (x1000 to x70000) shows the PVDF^{f}-TiO_2 after being submitted to three consecutive centrifugations. It is possible to observe similar surface coverage when comparing with Figure 4.9, which supports the suggestion that TiO_2 has a strong electrostatic attraction to the polymer.

In figure 4.22, on magnification x35000 and x70000 is it possible to verify the size of the TiO_2 nanoparticles which are within the range of 21.96 to 49.41 nm.

This is in agreement with the supplier AEROXIDE® DEGUSSA TiO_2 P25 which reports an average primary nanoparticle size of 21 nm.

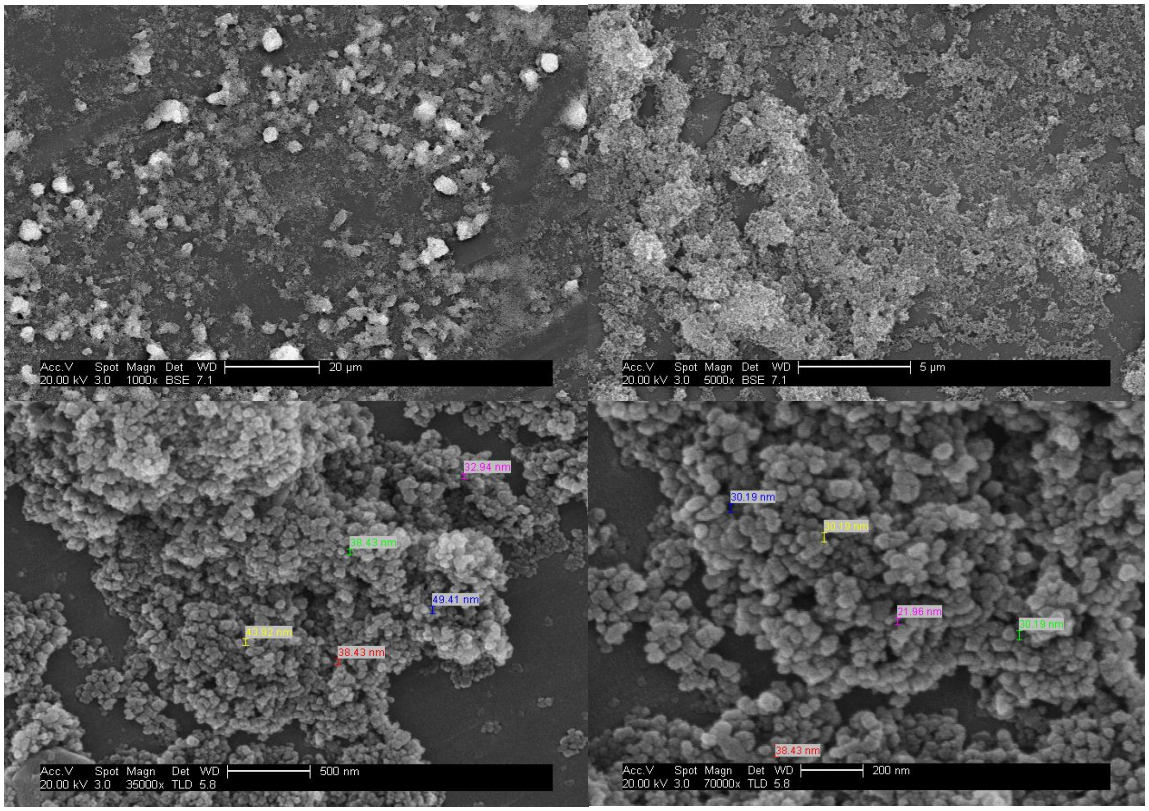

Figure 4.22- Surface analysis of PVDF^f- TiO2 (1.5 g / L prepared at pH = 3) and after three centrifugations. Clockwise from top left: a) x1000 b) x5000 c) x35000 d) x70000.

After three centrifugations the media shows the same order of kinetic (Figure 4.23) with the rate ranging from 0.0340 to 0.0311 min^{-1} and similar half-life times of 20.28 to 22.28 min, respectively. Table 4.2 lists the apparent first-order rate constants (K_{app}) and half-life for MB degradation after three consecutive centrifugations. Based on this media performance is it possible to confirm the strong electrostatic bond between TiO_2 and PVDF, which allowed continuing with adsorption experiments.

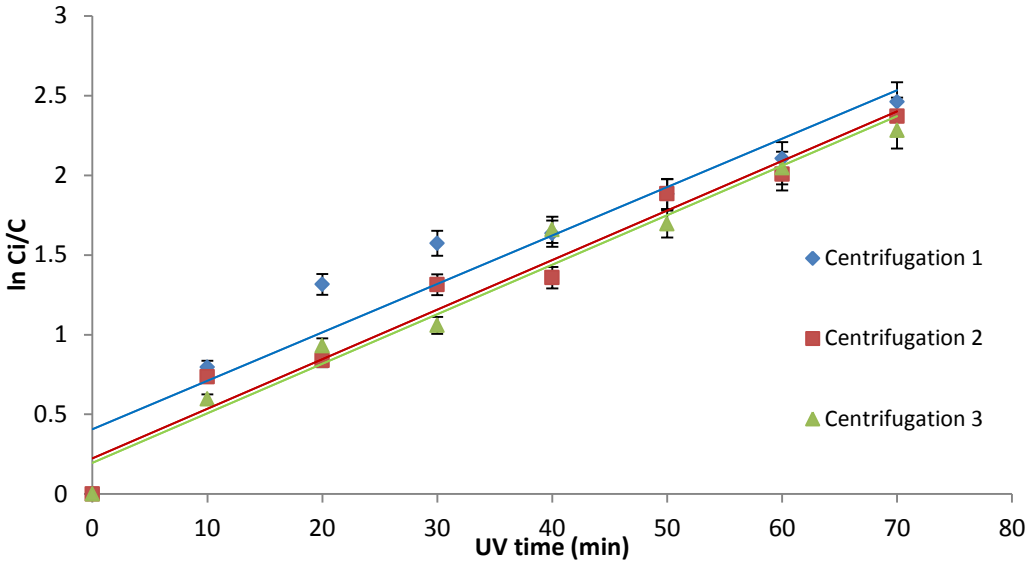

Figure 4.23– Pseudo-first order kinetics – PVDF^{f}-TiO$_2$ after three consecutive centrifugations

Table 4.2 - Photodegradation % and Pseudo-first-order kinetics parameters

PVDF^{f} – TiO$_2$	pH	[TiO$_2$]g/L	% Methylene Blue Photodegradation	Kapp (min^{-1})	R^2	t ½ (min)
Centrifugation 1	3	1.5	91.46	0.0340	0.9168	20.38
Centrifugation 2			90.64	0.0311	0.9654	22.28
Centrifugation 3			89.79	0.0311	0.9706	22.28

4.2.3. Blanks

In Figure 4.24, it is possible to observe the following blank tests:

a) PVDF pellets and MB expose to UV light;

b) PVDF pellets and MB in the dark;

c) PVDF^{f}-TiO$_2$ and MB in the dark;

The blanks experiments (Figure 4.24) shows that, without the addition of a photocatalyst (TiO$_2$) the percentage of photodegradation of MB is negligible and the UV light is the main responsible for the activation the electron-holes recombination of the catalyst, following by photocatalytic degradation.

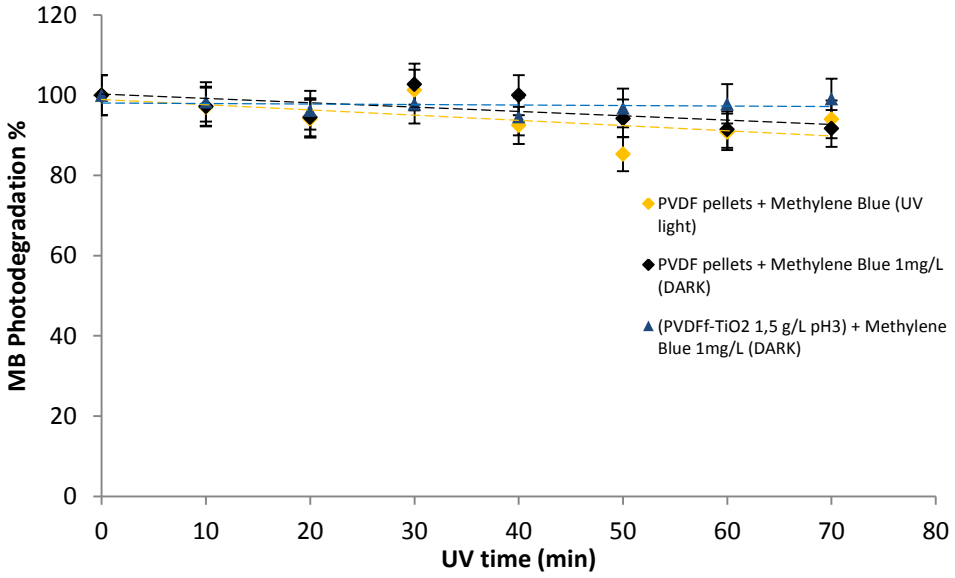

Figure 4.24– Blanks tests to assess the photocatalytic capacity of the media PVDF^{f}-TiO_2

To evaluate the PSFD reaction, PVDF and TiO_2 was prepared in the dark (absence of UV light) and the photodegradation capacity to degrade methylene blue assessed, following by centrifugations in between photodegradation reactions. In figure 4.25 it is possible to observe a successive decrease of the photodegradation rates. Figure 4.26-a) shows TiO_2 nanoparticles on the surface of the polymer. Even in the dark there is an electrostatic attraction between the TiO_2 and the surface of the polymer, but after three centrifugation tests in between (figure 4.16 b), the TiO_2 was mostly remove from the surface of the polymer.

According to this blank test, it is possible to confirm the importance of UV light in the photocatalytic surface functionalization deposition of TiO_2 onto PVDF surface, taking into account the mechanism suggested in figure 4.13.

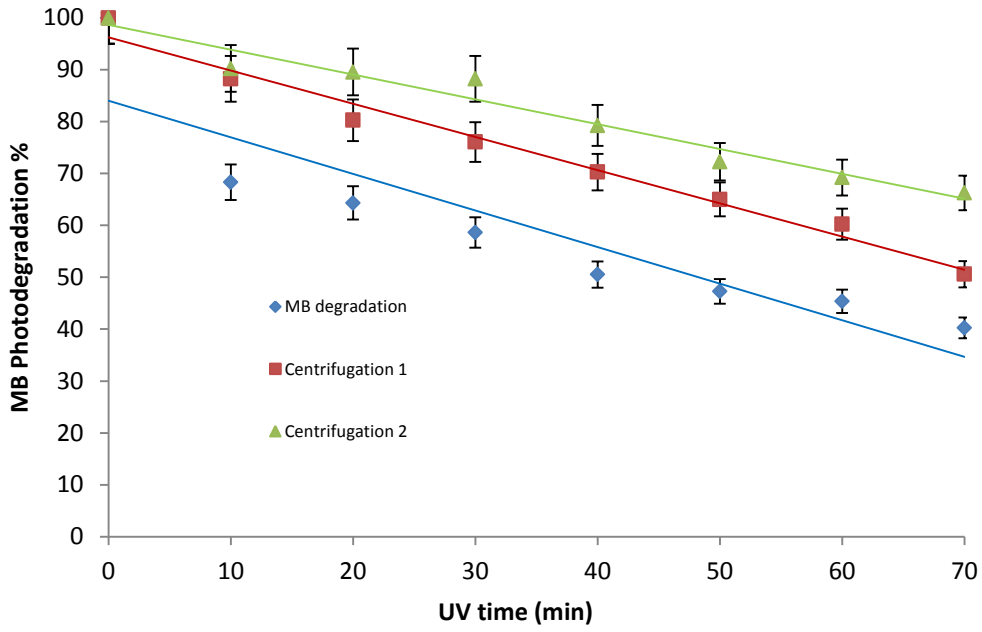

Figure 4.25 –Photodegradation capacity of PVDF +TiO_2 (1.5 g / L pH = 3) a) prepared without UV light (dark); b) and subjected to three consecutive centrifugations.

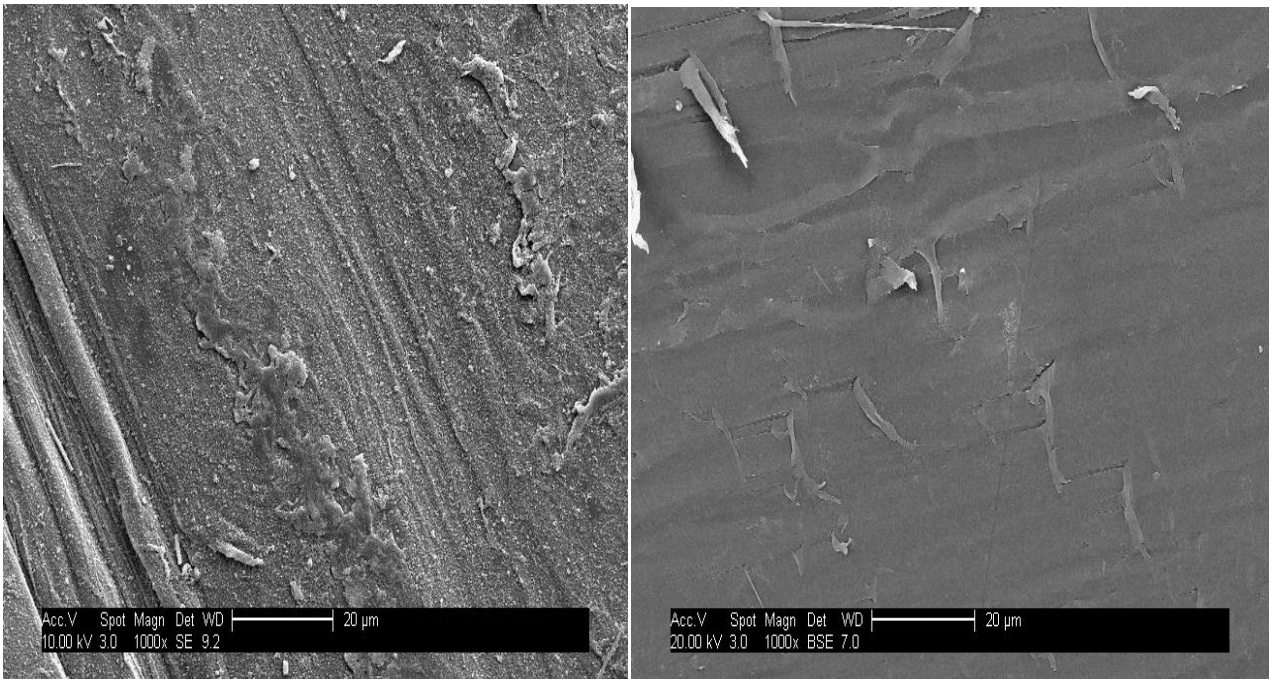

a) **b)**

Figure 4.26– Surface Analysis of PVDF + TiO_2 (1.5 g / L at pH = 3) a) prepared without UV light; b) subjected to three centrifugations

4.3. Humic acid adsorption

4.3.1. Adsorption isotherm of humic acid on TiO_2 powder

The adsorption isotherm for HA on TiO_2 powder is plotted in figure 4.27.

Based on the correlation coefficient (R^2), the adsorption of HA on TiO_2 follows a Langmuir model (figure 4.28) (Gürboğa and Tel 2005);(Nagaveni et al., 2004)

Langmuir parameters were calculated using equation 1.8 and reported in Table 4.3.

The value of maximum adsorption capacity (q_{max}) for HA adsorption using TiO_2 was 23.26 mg/g which is in agreement with the value reported by Wiszniowski, et al., (2003) of 20.52 mg/g.

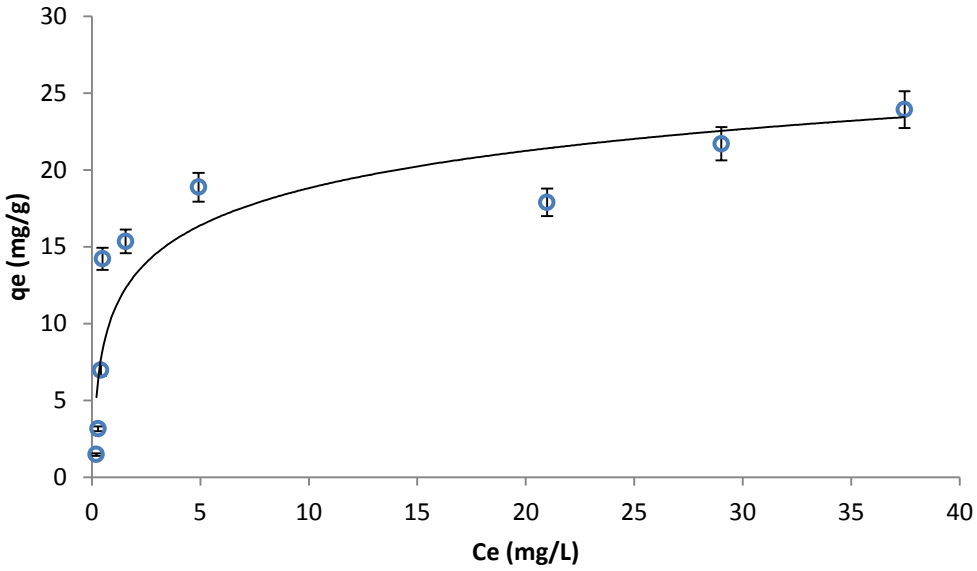

Figure 4.27– Adsorption isotherm of HA on TiO_2 at pH 5; qe (mg/g) is the concentration of HA adsorbed per gram of TiO_2 determined by UV-Vis spectroscopy at 254 nm; Ce (mg/L) is mass concentration of HA at the equilibrium, according to the Langmuir model

Table 4.3 – Adsorption constants for humic acid on TiO_2 according to the Langmuir model

Langmuir		
q_m (mg/g)	*b* (L/mg)	R^2
23.26	0.58	0.9803

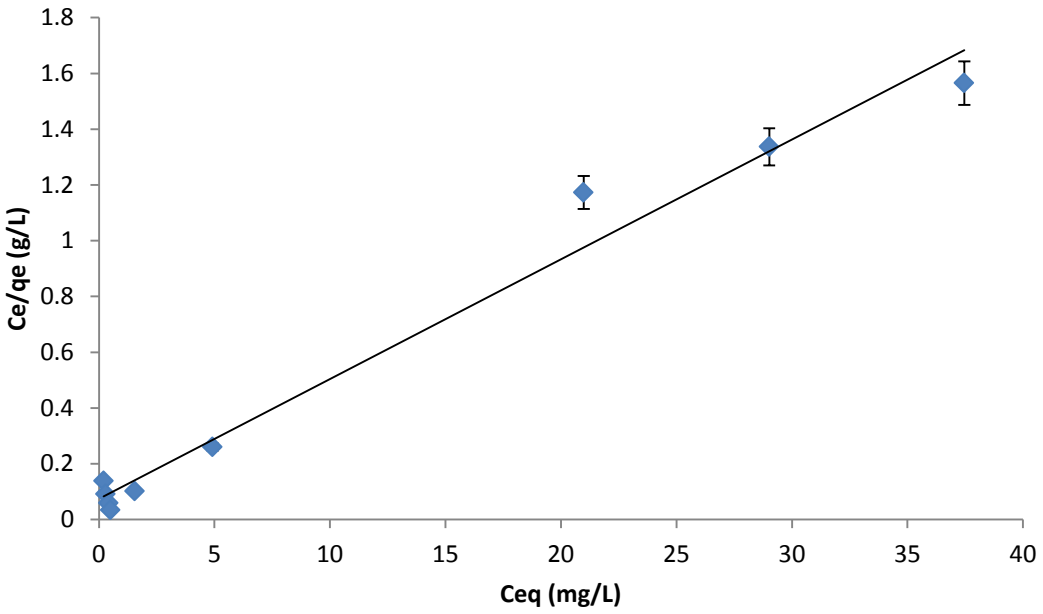

Figure 4.28–Linear plot of Langmuir isotherm for adsorption of HA onto PVDF^f-TiO$_2$

4.3.2. Adsorption isotherm of humic acid on PVDF^f - TiO$_2$ media prepared with optimized conditions (1.5 g/L, pH=3)

Since photocatalysis is a surface phenomenon, a critical step in intervening in the effectiveness of the photodegradation of a given pollutant is to understand the adsorption process of this pollutant on the catalyzing surface. Studying the adsorbability of the organic substrate allows one to predict the mechanism and kinetics that promote the pollutants photoxidation (Tachikawa et al.,2007).

The Langmuir and Freundlich isotherms, which were the most commonly employed models, were selected to describe the adsorption isotherms. The corresponding parameter values and correlation coefficients are presented in table 4.4. Based on the correlation coefficients (R^2), the adsorption of HA on PVDF^f-TiO$_2$ can be explained by both the Langmuir and Freundlich models.

4.3.2.1. Langmuir Isotherm

Figure 4.29 shows the experimental equilibrium isotherm for the adsorption of HA on PVDF^f-TiO$_2$ follows a Langmuir model. The linear plot of the specific adsorption (Ce/qe) against the equilibrium concentration (Ce) is plotted in figure 4.30. Using the Langmuir constant (b), a dimensionless constant termed as separation factor (R_L) could be calculated according to Equation 1.9. In Table 4.5 are reported the R_L values obtained for the different initial concentrations used in the adsorption studies. The values are below 1, demonstrating a

favorable adsorption of humic acid on PVDF^f-TiO_2 surface (Dutta et al., 2009).

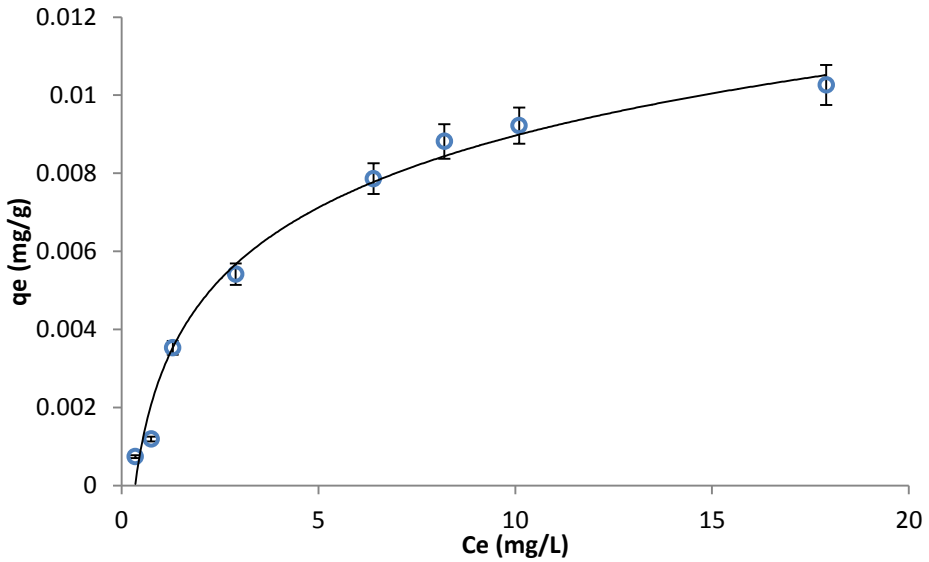

Figure 4.29–Adsorption isotherm of HA on PVDF^f - TiO_2; qe (mg/g) is the concentration of HA adsorbed per gram of PVDF^f - TiO_2 determined by UV-Vis spectroscopy at 254 nm; Ce (mg/L) is HA mass concentration at the equilibrium according to the Langmuir model

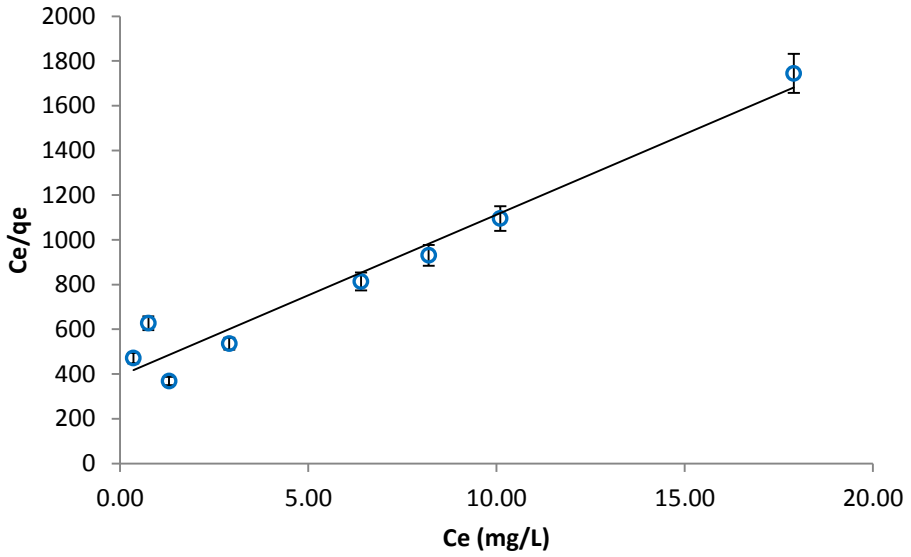

Figure 4.30– Linear plot of Langmuir isotherm for adsorption of HA onto PVDF^f-TiO_2

4.3.3.2. Freundlich Isotherm

The Freundlich isotherm was introduced as an empirical model, commonly used to describe the adsorption characteristics for heterogeneous surface. (Wan Ngah, et al., 2008)

Freundlich equilibrium constants were determined from the plot of log q_e versus log C_e (Figure 4.31), on the basis of the linear form of the Freundlich model (Equation 1.11)

Freundlich constants, K_f and *n* correspond to the adsorption capacity and adsorption intensity, respectively. The higher the value of K_f is, the higher is the adsorbent loading that can be achieved. In this case the low K_f (0.0019 L/mg) indicates that there is a low quantity of TiO_2 on the surface. The *n* value indicates the degree of nonlinearity between solution concentration and adsorption, as follows: if $n=1$, then adsorption is linear; if $n<1$, then adsorption is a chemical process; if $n>1$, then adsorption is a physical process. The *n* value in the Freundlich equation was found to be 1.44, (Table 4.4). The situation $n>1$ is the most common and may be due to a distribution of surface sites or any factor that causes a decrease in adsorbent-adsorbate interaction with increasing surface density values of *n* within the range of 1–10 represent favorable adsorption (Doulia et al., 2009);(Dutta et al., 2009);(Gürboğa and Tel., 2005);(Tahiri Alaoui et al., 2009).

In the present study, since *n* lies between 1 and 10 it indicates the physical adsorption of HA into $PVDF^f$-TiO_2. From the data in table 4.4, it can be seen that the value of $1/n = 0.695$ while $n = 1.44$ indicating that the adsorption of HA on $PVDF^f$-TiO_2 is favorable with a R^2 value is 0.9259.

The constant related to the affinity of the binding sites (b) is 0.184 L/mg and the adsorption intensity (1/n) is 0.695, implying that the distribution of TiO_2 on the surface of PVDF is even (Doulia et al. 2009) (Dutta et al. 2009)(Tahiri Alaoui et al. 2009).

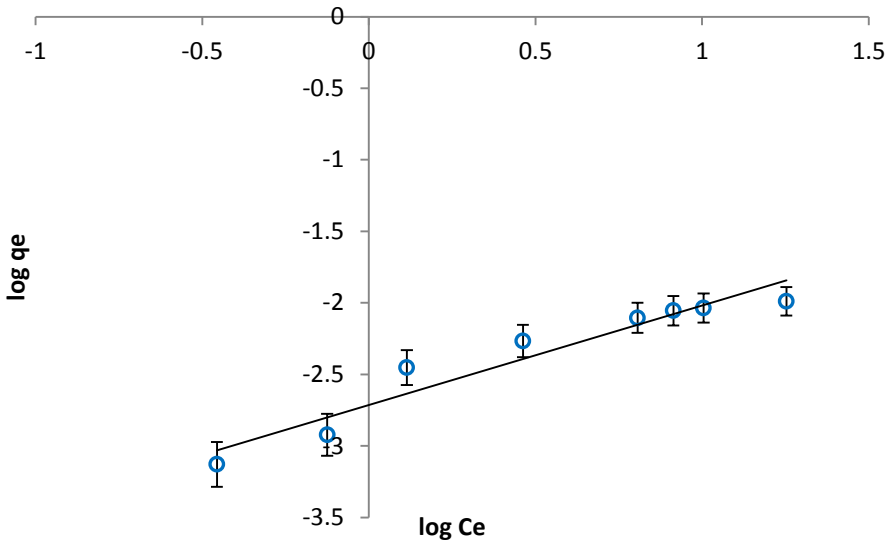

Figure 4.31– Linear plot of Freundlich isotherm for adsorption of HA onto PVDF^f-TiO$_2$

The value of maximum adsorption capacity (q_m) for HA adsorption into PVDF^f-TiO$_2$ was 0.0139 mg/g (Table 4.4) This value was much lower than 0.9877 mg/g of HA adsorption on TiO$_2$/activated carbon composites (Xue et al., 2011) and 23.26 mg/g in TiO$_2$ powder (Table 4.3). However, it cannot be accurately compared because PVDF^f-TiO$_2$ prepared in this study is not a powder type unlike other adsorbents. The adsorption of humic acid onto PVDF^f-TiO$_2$ is dependent upon the surface charge, hydrophobicity, and pore structure of the substrate and solutions conditions (Bekbolet et al., 2002);(Sun & Lee, 2012).

Table 4.4– Langmuir and Freundlich constants and regression coefficients for the adsorption of humic acid on the surface of PVDF^f-TiO$_2$

Langmuir			**Freundlich**			
q_m (mg/g)	*b* (L/mg)	R^2	Kf (L/mg)	1/n	n	R^2
0.0139	0.1840	0.9548	0.0019	0.6952	1.44	0.9259

Table 4.5 –Dimensionless Constant separation factor R_L for the adsorption of HA on PVDF^f-TiO_2

HA Initial Concentration (mg/L)	R_L
0.5	0.426
1.0	0.371
2.0	0.295
4.0	0.209
8.0	0.132
10.0	0.112
12.0	0.097
20.0	0.063

4.3.3. Calculation of the mass TiO_2 per gram of PVDF based on adsorption capacities

Based on the adsorption capacities for HA on TiO_2 and PVDF^f-TiO_2, it was estimated that the mass of TiO_2 nanoparticles per gram of PVDF, should be approximately 0.813 mg of TiO_2 per gram of PVDF (Table 4.6)

Table 4.6–Mass of TiO_2 (mg) per gram of PVDF

q_{max} (TiO_2) (mg/g)	q_{max} (PVDF^f-TiO_2 (mg/g)	Mass of TiO_2 (mg per gram of PVDF)
23.2601	0.0139	0.8130

However there is a work ongoing to exactly determine the exact thickness and amount of TiO_2 on the PVDF surface using EDX (Energy dispersive x-ray)(Ling, Mohamed, and Bhatia 2004).

4.3.4. Blanks

The blanks experiments, Figure 4.32 shows no adsorption of HA into either the PVDF pellets or the 0.22 µm filter units.

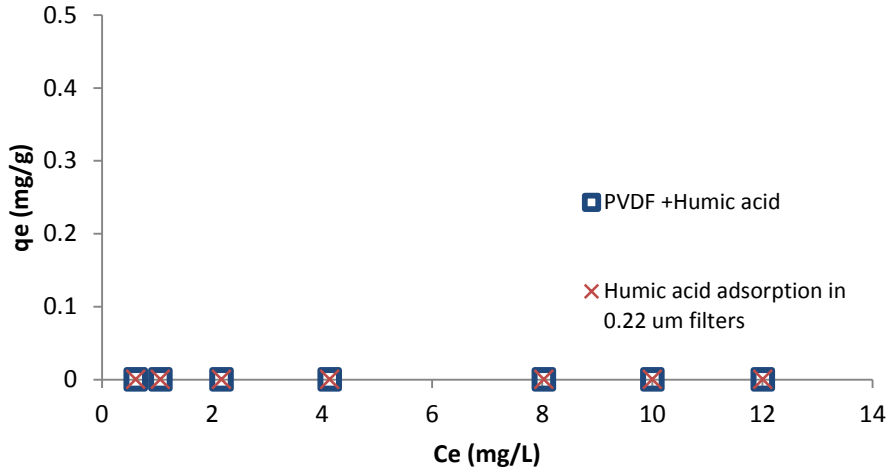

Figure 4.32 –Adsorption of humic acid in PVDF polymer pellets and 0,22µm filters

4.5. Photodegradation and adsorption of humic acid in PVDF^{f} - TiO_2 media

4.5.1. Determination of regeneration time

The aim of this determination was to determine a specific time to regenerate PVDF^{f}-TiO_2 by UV-V light under the collimated beam, after HA adsorption and thus be re-used in a fixed-bed adsorption column. Figure 4.33 shows the degradation decay curve of HA using the PVDF^{f} –TiO_2 media. At 120 minutes is it possible to observe 70 to 80% of degradation of HA, based on expressed results. This time was used as the regeneration time**.**

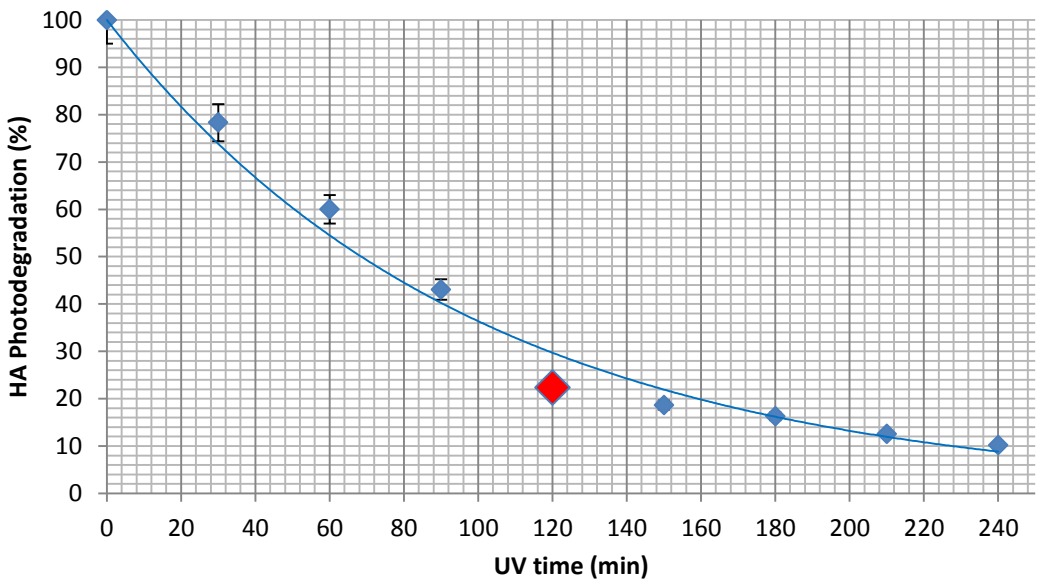

Figure 4.33– Photodegradation of humic acid with PVDF^f-TiO$_2$ media

Baek et al. (2013) report a schematic illustration for adsorption and photocatalytic degradation of HA by meso-TiO$_2$/SAC. This illustration (Figure 4.34) could also represent the adsorption mechanism and photocatalytic degradation of HA by PVDF^f-TiO$_2$. In the scheme it is possible to observe the HA adsorption on the surface and within the pores (in this case there are meso – TiO$_2$/SAC in the inside) and then the media submitted to UV-V light, where HA is oxidized to smaller compounds until completely mineralization. With this process is possible to regenerate the media for the next adsorption.

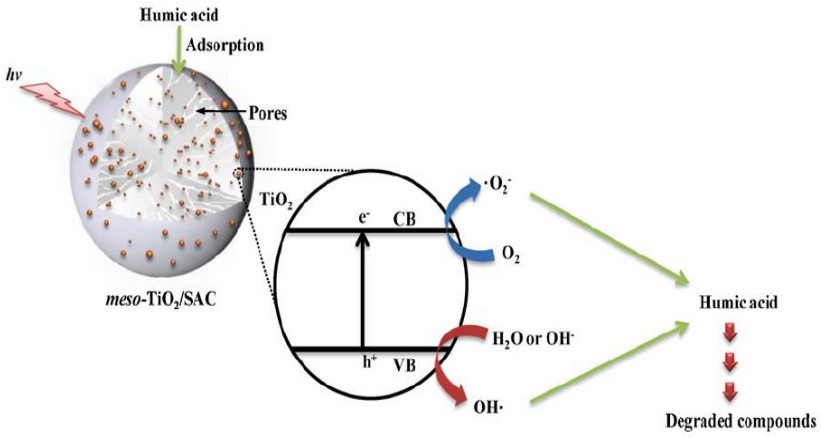

Figure 4.34 – Schematic illustration of the possible structure of meso – TiO$_2$/SAC and adsorption and photocatalytic degradation of HA by meso – TiO$_2$/SAC (Baek et al., 2013)

4.5.2. PVDF^{f}- TiO_2 Adsorption stability

The aim of this determination was to determine the stability and capacity of PVDF^{f}-TiO_2 to adsorb HA. Using the regeneration time determined in 4.5.1 it was possible regenerated the media, maintaining the adsorption capacity and stability.

Figure 4.35 shows the adsorption isotherms of HA on PVDF^{f}-TiO_2 replicated 8 times with 120 minutes regeneration time between adsorptions. It is possible to observe a similar Langmuir isotherm shape, indicating the stability of HA adsorption. In Figure 4.36 is shown the constancy of adsorption capacity per cycle, with an average value of 0.0140 mg/g. These results were an important base for developing a fixed-bed adsorption column in a laboratory pilot scale.

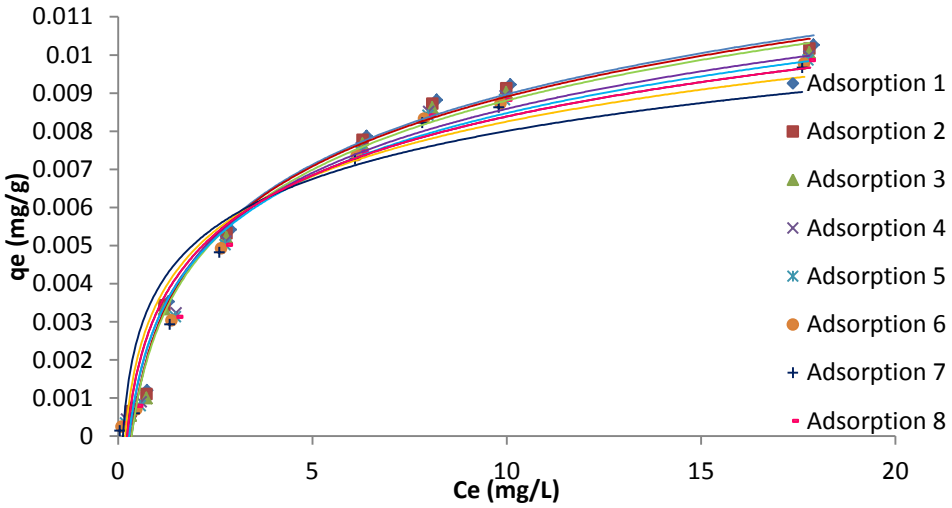

Figure 4.35 – Adsorption isotherms stability of HA on PVDF^{f}-TiO_2 showing 8 cycles with 120 min regeneration time per cycle

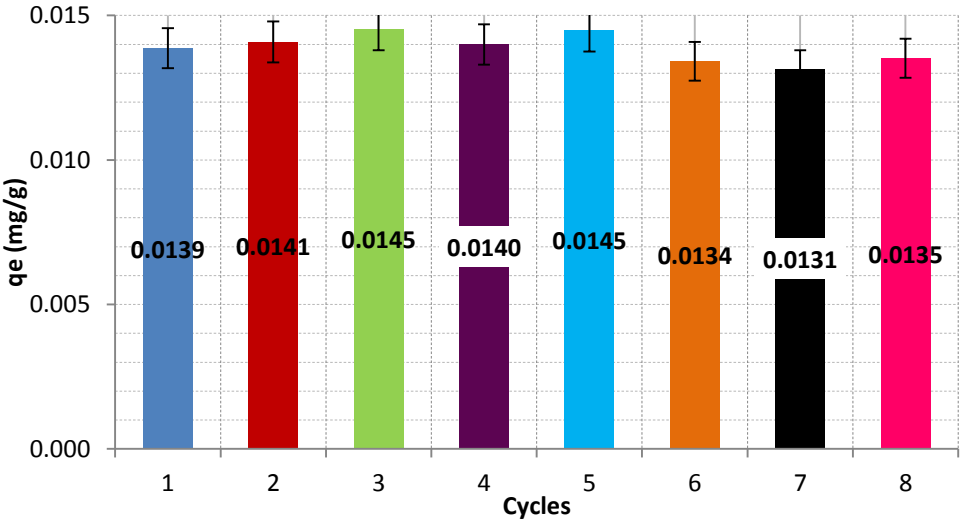

Figure 4.36 - Adsorption capacity of PVDF^{f}- TiO_2 showing 8 cycles with 120 minutes regeneration time per cycle

4.6. Adsorption column

Flow rate is an important parameter in evaluating the performance of an adsorption process, particularly for the continuous treatment of wastewater on industrial scale (He et al., 2010).

The operation and behavior of the continuous column adsorption can be determined by using the time to reach breakthrough and the shape of the breakthrough curve. The breakthrough curves show the loading behavior of HA in a continuous column and are usually expressed in terms of the normalized concentration, defined as the ratio of the outlet concentration (C) to the inlet concentration (C_0) as a function of time (in minutes)(He et al., 2010)(Mascolo et al., 2007)(Qi & Schideman, 2008)(Yu et al., 2012)

Therefore, the effect of flow rate on adsorption of HA by PVDF^f-TiO_2 was studied by varying the flow rates from 1.30 to 10.4 mL/min and keeping the initial HA concentration of 5 mg/L and the bed height (17 cm) constant.

The effect of the flow rate on the breakthrough performance at the above operating conditions for PVDF^f-TiO_2 is shown in Figure 4.37. From the figure it can be seen that the breakthrough time as well as the adsorption efficiency of PVDF^f-TiO_2 was lower at a higher flow rate. As the flow rate increased from 1.30 to 10.40 mL/min, the saturation time decreased from 410 to 140 min (Table 4.7). This is due to the fact that at higher flow rate the contact time of the HA with the PVDF^f-TiO_2 surface is very short, and hence the HA molecules do not have enough time to capture the binding sites on the PVDF^f-TiO_2 surface, leaving the column before equilibrium occurs (Goetz et al. 2009).

However, the breakthrough curve became steeper when the flow rate was increased which caused a decrease on the breakthrough time and the HA removal efficiency. However, when the flow rates were low, according with He et al. (2010) and Mascolo et al. (2007), the external mass transfer controlled the process and it was also ideal for intra particle diffusion system. Thus, the lower the flow rates, the more effective was the adsorption process and higher was the residence time of the adsorbate, which ultimately resulted in a better adsorption capacity (Yu et al. 2012).

The highest HA removal (0.42%) was recorded when the flow rate was 1.30 mL/min. When the inlet flow rate increased from 1.30 mL/min to 10.40 mL/min, the removal decreased from 0.42 % to 0.16 % (Table 4.7).

Due the low values of HA removal, the testing of lower feed concentrations of HA and also an increase the EBCT are recommended for further work.

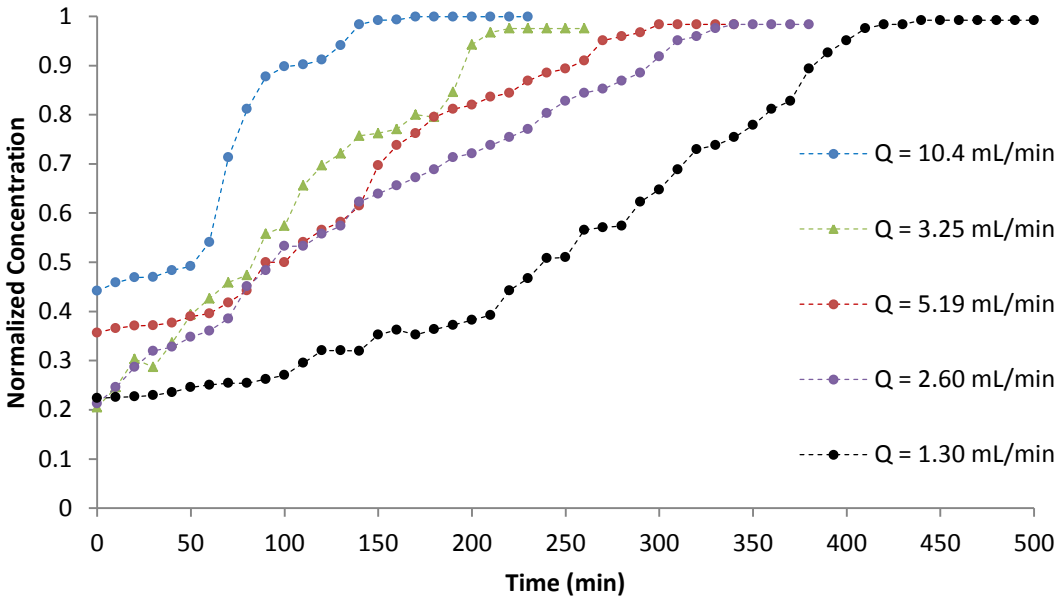

Figure 4.37- Breakthrough curves of HA on PVDF^f-TiO_2

Table 4.7 – Saturation times and total removals in fixed-bed adsorption column

F (mL/min)	EBCT (min.)	Saturation times (min.)	Total mass of HA through the column (mg)	Total removal %
10.40	62.9	140	7.28	0.16
5.19	126.0	200	5.19	0.22
3.25	201.3	270	4.39	0.26
2.60	251.6	310	4.03	0.28
1.30	503.3	410	2.66	0.42

5. Conclusion

This work presents an innovative and simple way to prepare a highly photoactive catalyst combining TiO_2 and PVDF polymeric pellets, by photocatalytic surface functionalization deposition ($PVDF^f$-TiO_2).

The surface of the new media $PVDF^f$-TiO_2 shows that the PSFD treatment induced simultaneous surface functionalization involving oxygen-surface species formation and deposition of TiO_2 on carboxylic groups due to an electrostatic attraction.

The TiO_2 deposition occurred preferentially when pH<7 and the activity of photocatalyst increased with acidity during PSFD treatment;

The optimized conditions to prepare $PVDF^f$-TiO_2 is a solution of 1.5 g/L of TiO_2 (pH 3), according with the % methylene blue photodegradation, K_{app} and $t_{1/2}$ expressed on table 4.1.

The $PVDF^f$-TiO_2 prepared in optimized conditions, shows a capacity to adsorb HA with a q_{max} of 0.0139 mg/g and be generated by 70-80% in 120 minutes under UV exposure. The fixed-bed adsorption column packed with $PVDF^f$-TiO_2 shows a removal of 0.42% of HA solution (5 mg/L) with the lowest flow rate (1.30 mL/min).

6. Suggestions for future work

Several topics related to the above work remain to be explored. Thus, in this page some future research developments that can be followed in a near opportunity are mentioned:

Media Preparation:

- Evaluate different types of fluoropolymers for the PSDF reaction;
- Evaluate different form types of TiO_2;
- Assess different UV exposures times to extend the PSFD reaction;
- Relate the UV energy light with the extent of reaction;
- Evaluate the thickness and amount of TiO_2 on the polymers surface by EDX (ongoing work);
- Understand and develop a better knowledge about the mechanism of PSFD;

Media Performance:

- Evaluate the media for adsorption of other contaminants in water;
- Evaluate the media for use in a continuous photo-reactor to mineralize compounds that are dangerous to the environment;
- Combine media with different adsorbents to remove pollutants from water;
- Optimize media for higher adsorption capacity;

Adsorption column:

- Test different feed concentrations of HA or other pollutants;
- Test different EBCT;
- Evaluate different types of columns;
- Determine TOC and THMFP from the effluent;

A scale-up study to step up from the laboratory prototype to an industrial stage should be performed. Finally, an economic analysis and a life cycle assessment of all the treatment process studied for application in an industrial scale after all the optimization should be made.

7. References

Andreozzi, R., Caprio, V., Insola, A., and Marotta, R.. 1999. "Advanced Oxidation Processes (AOP) for Water Purification and Recovery" 53: 51–59.

Baek, M., Yoon, J., Hong, J., and Suh, J.. 2013. "Application of TiO_2-Containing Mesoporous Spherical Activated Carbon in a Fluidized Bed photoreactor—Adsorption and Photocatalytic Activity." *Applied Catalysis A: General* 450 (January). Elsevier B.V. 222–29.

Banerjee, P., Dasgupta, S., and De, S. 2007. "Removal of Dye from Aqueous Solution Using a Combination of Advanced Oxidation Process and Nanofiltration." *Journal of Hazardous Materials* 140 (1-2): 95–103.

Bayarri, B., Abellán, M.N., Giménez, J., and Esplugas, S. 2007. "Study of the Wavelength Effect in the Photolysis and Heterogeneous Photocatalysis." *Catalysis Today* 129 (1-2): 231–39.

Bekbolet, M., Suphandag, A. S.,and Uyguner, C.S. 2002. "An Investigation of the Photocatalytic Efficiencies of TiO_2 Powders on the Decolourisation of Humic Acids" 148: 121–28.

Bizani, E., Fytianos, K., Poulios, I., and Tsiridis, V. 2006. "Photocatalytic Decolorization and Degradation of Dye Solutions and Wastewaters in the Presence of Titanium Dioxide." *Journal of Hazardous Materials* 136 (1): 85–94.

Bundaleski, N., Silva, A.G., Schröder, U., Moutinho, A.M.C., and Teodoro, O.M.N.D. 2010. "Adsorption Dynamics of Water on the Surface of TiO2 (110)." *Journal of Physics: Conference Series* 257 (November): 012008.

Carvalho, H.W.P, Batista, A.P.L, Hammer, P., Ramalho, T.C.. 2010. "Photocatalytic Degradation of Methylene Blue by TiO2-Cu Thin Films: Theoretical and Experimental Study." *Journal of Hazardous Materials* 184 (1-3). Elsevier B.V. 273–80.

Chang, H., Su, C., Lo, C.H., Chen, L.C., Tsung, T.T. and Jwo, C.S.. 2004. "Photodecomposition and Surface Adsorption of Methylene Blue on TiO_2 Nanofluid Prepared by ASNSS" 45 (12): 3334–37.

Chen, C., Wang, X., Jiang, H., and Hu, W. 2007. "Direct Observation of Macromolecular Structures of Humic Acid by AFM and SEM." *Colloids and Surfaces A: Physicochemical and Engineering Aspects* 302 (1-3): 121–25.

Chen, Q., Yin, D., Zhu, S., and Hu, X. 2012. "Adsorption of cadmium(II) on Humic Acid Coated Titanium Dioxide." *Journal of Colloid and Interface Science* 367 (1). Elsevier Inc. 241–48.

Doulia, D., Leodopoulos, C., Gimouhopoulos, K., and Rigas, F. 2009. "Adsorption of Humic Acid on Acid-Activated Greek Bentonite." *Journal of Colloid and Interface Science* 340 (2). Elsevier Inc. 131–41.

Dutta, S., Parsons, S.a., Bhattacharjee, C., Jarvis, P., Datta, S. , and Bandyopadhyay, S. 2009. "Kinetic Study of Adsorption and Photo-Decolorization of Reactive Red 198 on TiO2 Surface." *Chemical Engineering Journal* 155 (3): 674–79.

El-Sharkawy, E., Soliman, A.Y., and Al-Amer, K.M . 2007. "Comparative Study for the Removal of Methylene Blue via Adsorption and Photocatalytic Degradation." *Journal of Colloid and Interface Science* 310 (2): 498–508.

Goetz, V., Cambon, J.P., Sacco, D. , and Plantard, G. 2009. "Modeling Aqueous Heterogeneous Photocatalytic Degradation of Organic Pollutants with Immobilized TiO2." *Chemical Engineering and Processing: Process Intensification* 48 (1): 532–37.

Gómez-Solís, C., Juárez-Ramírez, I., Moctezuma, E., and Torres-Martínez, L.M. 2012. "Photodegradation of Indigo Carmine and Methylene Blue Dyes in Aqueous Solution by SiC-TiO2 Catalysts Prepared by Sol-Gel." *Journal of Hazardous Materials* 217-218 (May). Elsevier B.V. 194–99.

Gupta, V. K., Carrott, P. J.M., and Ribeiro Carrott, M.M.L. 2009. "Low-Cost Adsorbents: Growing Approach to Wastewater Treatment—a Review." *Critical Reviews in Environmental Science and Technology* 39 (10): 783–842.

Gürboğa, G., and Tel, H. 2005. "Preparation of TiO_2-SiO_2 Mixed Gel Spheres for Strontium Adsorption." *Journal of Hazardous Materials* 120 (1-3): 135–42.

He, J., Hong, S., Zhang, L., Gan, F., and Ho, Y.S. 2010. "Equilibrium and Thermodynamic Parameters of Adsorption of Methylene Blue onto Rectorite." *Fresenius Environmental Bulletin* 19 (11): 2651–56.

Houas, A., Lachheb, H., Ksibi, M., Elaloui, E., Guillard, C., and Herrmann, J.M.. 2001. "Photocatalytic Degradation Pathway of Methylene Blue in Water" 31: 145–57.

Hristovski, K., Baumgardner, A., and Westerhoff, P. 2007. "Selecting Metal Oxide Nanomaterials for Arsenic Removal in Fixed Bed Columns: From Nanopowders to Aggregated Nanoparticle Media." *Journal of Hazardous Materials* 147 (1-2): 265–74.

Humbert, H., Gallard, H., Suty, H., and Croué, J.P.. 2008. "Natural Organic Matter (NOM) and Pesticides Removal Using a Combination of Ion Exchange Resin and Powdered Activated Carbon (PAC)." *Water Research* 42 (6-7): 1635–43.

Hwang, K.J., Lee, J.W., Shim, W.G., Jang, H.D., Lee, S.I., and Yoo, S.J. 2012. "Adsorption and Photocatalysis of Nanocrystalline TiO_2 Particles Prepared by Sol–gel Method for Methylene Blue Degradation." *Advanced Powder Technology* 23 (3). The Society of Powder Technology Japan: 414–18.

Kaewprasit, C., Hequet, E., Abidi, N., and Gourlot, J.P. 1998. "Application of Methylene Blue Adsorption to Cotton Fiber Specific Surface Area Measurement: Part I. Methodology" 173: 164–73.

Kasanen, J., Salstela, J., Suvanto, M., and Pakkanen, T.T. 2011. "Photocatalytic Degradation of Methylene Blue in Water Solution by Multilayer TiO_2 Coating on HDPE." *Applied Surface Science* 258 (5). Elsevier B.V. 1738–43.

Khezrianjoo, S, and Revanasiddappa, H.D. 2012. "Langmuir-Hinshelwood Kinetic Expression for the Photocatalytic Degradation of Metanil Yellow Aqueous Solutions by ZnO Catalyst Langmuir-Hinshelwood Kinetic Expression for the Photocatalytic Degradation of Metanil Yellow Aqueous Solutions by ZnO Catalyst" *Chemical Sciences Journal*, Vol.2012:CSJ-85

Kuo, W. S., and Ho, P.H. 2001. "Solar Photocatalytic Decolorization of Methylene Blue in Water." *Chemosphere* 45 (1): 77–83.

Li, Q., Yahong, Z., Wang, L., and Aiqin, W. 2011. “Adsorption Characteristics of Methylene Blue onto the N-Succinyl-Chitosan-G-Polyacrylamide/attapulgite Composite.” *Korean Journal of Chemical Engineering* 28 (8): 1658–64. .

Li, Y., Xiaodong, L., Junwen, L., and Jing,Y. 2006. “Photocatalytic Degradation of Methyl Orange by TiO2-Coated Activated Carbon and Kinetic Study.” *Water Research* 40 (6): 1119–26.

Ling, C., Abdul, R. M., and Subhash, B. 2004. “Performance of Photocatalytic Reactors Using Immobilized TiO2 Film for the Degradation of Phenol and Methylene Blue Dye Present in Water Stream.” *Chemosphere* 57 (7): 547–54.

Mascolo, G, Comparelli, R, Curri,M.L, Lovecchio,G., Lopez,A. and Agostiano, A. 2007. “Photocatalytic Degradation of Methyl Red by TiO_2: Comparison of the Efficiency of Immobilized Nanoparticles versus Conventional Suspended Catalyst.” *Journal of Hazardous Materials* 142 (1-2): 130–37.

Matilainen, A., Lahtinen, T., Hed, L.,Bhatnagar,A. and Sillanpää,M. 2011. “An Overview of the Methods Used in the Characterisation of Natural Organic Matter (NOM) in Relation to Drinking Water Treatment.”

Matilainen, A., and Sillanpää, M. 2010. “Removal of Natural Organic Matter from Drinking Water by Advanced Oxidation Processes.” *Chemosphere* 80 (4). Elsevier Ltd: 351–65.

Mazille, F., Lopez, A. and Pulgarin, C. 2009 a. “Synergistic Effect of TiO_2 and Iron Oxide Supported on Fluorocarbon Films.” *Applied Catalysis B: Environmental* 90 (3-4): 321–29.

Mazille, F., Schoettl, T. and Pulgarin, C.. 2009 b. “Synergistic Effect of TiO_2 and Iron Oxide Supported on Fluorocarbon Films. Part 1: Effect of Preparation Parameters on Photocatalytic Degradation of Organic Pollutant at Neutral pH.” *Applied Catalysis B: Environmental* 89 (3-4): 635–44.

Mori, M., Tsuyoshi, S., Akinori, M., Takahiro, F., Masaru, K., Shigekazu, K., Saito, Y., Ito, T., and Itabashi, H. 2013. “Photodecomposition of Humic Acid and Natural Organic Matter in Swamp Water Using a TiO(2)-Coated Ceramic Foam Filter: Potential for the Formation of Disinfection Byproducts.” *Chemosphere* 90 (4): 1359–65.

Nagaveni, K., Hegde, M.S., Ravishankar, N., Subbanna, G.N., and Madras, G. 2004. "Synthesis and Structure of Nanocrystalline TiO_2 with Lower Band Gap Showing High Photocatalytic Activity." *Langmuir : The ACS Journal of Surfaces and Colloids* 20 (7): 2900–2907.

Ngang, H.P., Ooi, B.S., Ahmad, A.L., and Lai, S.O. 2012. "Preparation of PVDF–TiO2 Mixed-Matrix Membrane and Its Evaluation on Dye Adsorption and UV-Cleaning Properties." *Chemical Engineering Journal* 197 (July): 359–67.

Oliveira, J., Silveira, L. 2011. "Utilização de Dióxido de Titânio Em Processos Fotocatalíticos Para Degradação de Halofenóis." *Vivencias: Revista Eletrônica de Extensão Da URI* 7: 91–104.

Páez, C.A., Lambert, S.D., Poelman, D., Pirard, J.P., and Heinrichs, B. 2011. "Improvement in the Methylene Blue Adsorption Capacity and Photocatalytic Activity of H2-Reduced Rutile-TiO2 Caused by Ni(II)porphyrin Preadsorption." *Applied Catalysis B: Environmental* 106 (1-2). Elsevier B.V. 220–27.

Park, H., Park, Y., Kim, W., and Choi, W. 2012. "Surface Modification of TiO2 Photocatalyst for Environmental Applications." *Journal of Photochemistry and Photobiology C: Photochemistry Reviews*, November. Elsevier B.V., 1–20.

Peng, H., Feng, S., Zhang, X., Li, Y., and Zhang, X. 2012. "Adsorption of Norfloxacin onto Titanium Oxide: Effect of Drug Carrier and Dissolved Humic Acid." *The Science of the Total Environment* 438 (November). Elsevier B.V. 66–71.

Prieto, O., Fermoso, J., Nuñez, Y., del Valle, J.L., and Irusta, R. 2005. "Decolouration of Textile Dyes in Wastewaters by Photocatalysis with TiO_2." *Solar Energy* 79 (4): 376–83.

Polymers Database 2013 [Internet] Copyright © 2014 Taylor & Francis Group, available at http://www.polymersdatabase.com/

Qi, S., and Schideman, L.C. 2008. "An Overall Isotherm for Activated Carbon Adsorption of Dissolved Natural Organic Matter in Water." *Water Research* 42 (13): 3353–60.

Senthilkumaar, S., Porkodi, K., Gomathi, R., Geetha Maheswari, A., and Manonmani, N. 2006. "Sol–gel Derived Silver Doped Nanocrystalline Titania Catalysed Photodegradation of Methylene Blue from Aqueous Solution." *Dyes and Pigments* 69 (1-2): 22–30.

Sauer, T., Cesconeto Neto, G., José, H.J., and Moreira, R. F. P. M. 2002. "Kinetics of Photocatalytic Degradation of Reactive Dyes in a TiO_2 Slurry Reactor" 149: 147–54.

Shen, C., Wang, Y.J., Xu, J.H., and Luo, G.S. 2012. "Facile Synthesis and Photocatalytic Properties of TiO2 Nanoparticles Supported on Porous Glass Beads." *Chemical Engineering Journal* 209 (October): 478–85.

Shimizu, N., Chiaki Ogino, Mahmoud Farshbaf Dadjour, and Tomoyuki Murata. 2007. "Sonocatalytic Degradation of Methylene Blue with TiO_2 Pellets in Water." *Ultrasonics Sonochemistry* 14 (2): 184–90.

Sofia, C. 2008. "Synthesis , Spectroscopy and Characterization of Titanium Dioxide Based Photocatalysts for the Degradative Oxidation of Organic Pollutants." Thesis for the Degree of Doctor of Philosophy in Chemical and Biological Engineering. Universidade do Porto, 2008.

Sun, D., Lee,P.F. 2012. "TiO_2 Microsphere for the Removal of Humic Acid from Water: Complex Surface Adsorption Mechanisms." *Separation and Purification Technology* 91 (May). Elsevier B.V. 30–37.

Tachikawa, T., Fujitsuka,M. and Majima,T. 2007. "Mechanistic Insight into the TiO 2 Photocatalytic Reactions : Design of New Photocatalysts". *Journal of Physical Chemistry* 111 (14): 37–39.

Tahiri A., Ouafa, B., Quang, T. N., Mbareck, C., and Rhlalou, T. 2009. "Elaboration and Study of Poly(vinylidene Fluoride)–anatase TiO_2 Composite Membranes in Photocatalytic Degradation of Dyes." *Applied Catalysis A: General* 358 (1): 13–20.

Uyguner, C.S., and Bekbolet, M.. 2004. "Photocatalytic Degradation of Natural Organic Matter : Kinetic Considerations and Light Intensity Dependence". *International Journal of Photoengergy* 6: 73-80.

Uyguner, C. S., and Bekbolet, M. 2011. "Significance of Analytical Parameters for the Understanding of Natural Organic Matter in Relation to Photocatalytic Oxidation." *Chemosphere* 84 (8). Elsevier Ltd: 1009–31.

Valente, J. P. S, Padilha, P.M, and Florentino, A.O. 2006. "Studies on the Adsorption and Kinetics of Photodegradation of a Model Compound for Heterogeneous Photocatalysis onto TiO(2)." *Chemosphere* 64 (7): 1128–33.

Wan-Ngah, W. S., Hanafiah, M. a. K. M. and Yong, S.S. 2008. "Adsorption of Humic Acid from Aqueous Solutions on Crosslinked Chitosan-Epichlorohydrin Beads: Kinetics and Isotherm Studies." *Colloids and Surfaces. B, Biointerfaces* 65 (1): 18–24.

Wiszniowski, J., Didier R, Surmacz-Gorska, J., Miksch, K., and Weber, J.V. 2003. "Photocatalytic Mineralization of Humic Acids with TiO_2 : Effect of pH , Sulfate and Chloride Anions" 5: 0–5.

Worch, E. 2012. *Adsorption Technology in Water Treatment - Fundamentals, Processes and Modeling*. Edited by Berlin/Boston Walter de Gruyter GmbH & Co. KG.

Xue, G., Liu, H., Chen, Q., Hills, C., Tyrer, M. and Innocent, F.. 2011. "Synergy between Surface Adsorption and Photocatalysis during Degradation of Humic Acid on TiO2/activated Carbon Composites." *Journal of Hazardous Materials* 186 (1). Elsevier B.V. 765–72.

Yates, J. T. 2009. "Photochemistry on TiO_2: Mechanisms behind the Surface Chemistry." *Surface Science* 603 (10-12): 1605–12.

Yu, J., Yu, H., Cheng, B., Zhou, M., and Zhao, X. 2006. "Enhanced Photocatalytic Activity of TiO2 Powder (P25) by Hydrothermal Treatment." *Journal of Molecular Catalysis A: Chemical* 253 (1-2): 112–18.

Yu, J.X., Chi, R.A., Guo, J., Zhang, Y.F., Xu, Z. and Xiao, C. 2012. "Desorption and Photodegradation of Methylene Blue from Modified Sugarcane Bagasse Surface by Acid TiO2 Hydrosol." *Applied Surface Science* 258 (8). Elsevier B.V. 4085–90.

Zhang, S., Chen, Z., L., Wang, Q., and Wan, L. 2008. “Photocatalytic Degradation of Methylene Blue in a Sparged Tube Reactor with TiO_2 Fibers Prepared by a Properly Two-Step Method.” *Catalysis Communications* 9 (6): 1178–83.

8. Annex

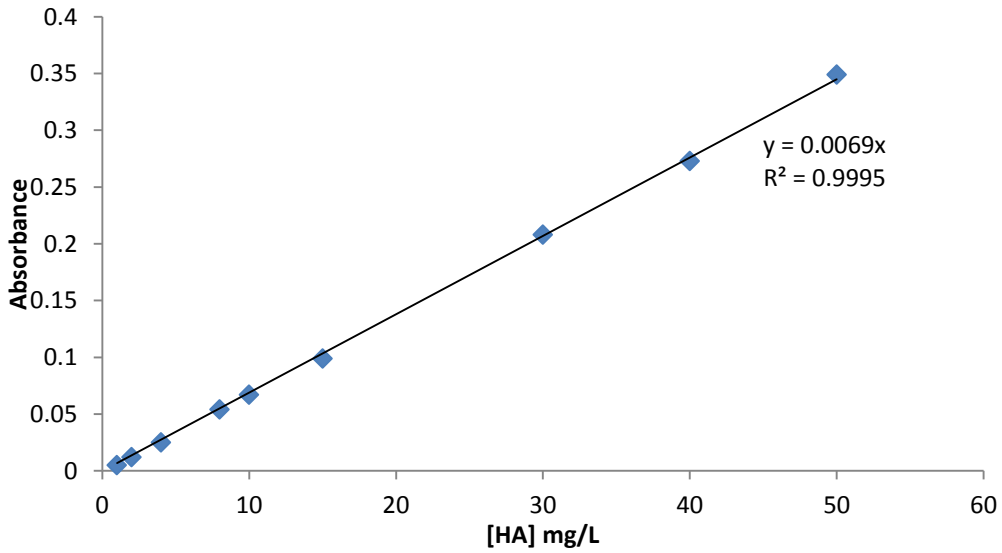

Figure 8.1 – Humic acid calibration curve